Current Derivative Based Fault Detection and Localization in a Ring Bus DC Microgrid

by

Yunfei Bai

A thesis submitted to the Faculty of Graduate Studies of

The University of Manitoba

in partial fulfillment of the requirements of the degree of

MASTER OF SCIENCE

Department of Electrical and Computer Engineering

University of Manitoba

Winnipeg, Manitoba

Abstract

This thesis investigates the protection aspects of a 400 V DC microgrid with a ring bus architecture. Based on the existing literature, a model of a simple ring bus DC microgrid was developed in PSCAD simulation software to understand the fault behavior and protection requirements. Protection related features such as grounding circuits and DC circuit breakers were also included in the model. Analytical expressions for the initial fault currents were developed considering simplified equivalent circuits. The expressions indicate that challenges of the DC microgrid protection are operation speed and selectivity. Based on these results, a combined protection scheme with two different protection concepts and settings procedures were proposed.

This proposed protection scheme divides DC microgrid faults into two categories: low resistance faults and high resistance faults. A current derivative protection method using local measurements was designed to detect the low resistance faults. A unit protection method using the ratio of current derivatives observed at two ends of the protected line was designed to detect the high resistance faults. The unit protection algorithm also allows the determination of fault locations. Various simulation results verified the operation of the proposed protection scheme as well as the fault location performance and showed that it satisfies speed and selectivity requirements of a typical low voltage DC microgrid. This research highlighted that using multiple protection methods cooperated together can significantly reduce the protection challenges and constraints in DC microgrids.

Acknowledgements

I would like to thank my academic advisor Dr. Athula Rajapakse for his teaching, guidance, encouragement and supervision throughout my graduate studies. With his guidance, I could develop good research skills and gain valuable and interesting knowledge related to renewable energy, DC distribution systems and power system protection.

I would like to thank Dr. Charles Adewola for his many valuable suggestions and assistances during the initial period of my research.

I would also like to thank Mr. Haleem Naushath who is currently a Ph.D. candidate for teaching me skills of PSCAD and sharing with me many important experiences in research studies.

Finally, I would like to sincerely thank my parents and friends who continuously supported me during my entire graduate program, and I will always remember the encouragement from all of you when I was having hard times.

Dedication

To my family

Contents

List of Tables

List of Figures

List of Abbreviations

ACMG	AC Microgrid
BMS	Battery Management System
CB	Circuit Breaker
CLI	Current Limiting Inductor
DC/DC	DC-to-DC
DCMG	DC Microgrid
DG	Distributed Generator
ESS	Energy Storage System
HRF	High Resistance Fault
LRF	Low Resistance Fault
MPPT	Maximum Power-Point Tracking
PD	Protective Device
PG	Pole-to-Ground
POC	Point of Connection
PP	Pole-to-Pole
PV	Photovoltaic

RES	Renewable Energy Source
SNR	Signal-to-Noise Ratio
SOC	State of Charge
VSC	Voltage Source Converter

Chapter 1 Introduction

1.1 Background

With the rapid growth of population, economy and urbanization, the electrical power demand increases dramatically. Currently, about 65% of the world's electrical energy is generated by thermal power plants [1]. The thermal power plants which burn fossil fuels have caused severe air pollution issues [2]. The global warming caused by their carbon dioxide emissions has also led to numerous issues such as melting of glaciers, seal level rise, and unprecedented extreme weather events. There is an urgent desire to replace fossil fuel based electricity generation with clean energy resources.

Renewable energy sources (RES) such as solar photovoltaics (PV) systems and wind turbines produce electricity without causing significant negative effects on the environment and ecological system [3]. To supplement the large-scale conventional electricity generation, electrical engineers have developed distributed generators (DGs) based on RES as additional power sources [4]. In recent years, the framework called microgrid has become a major approach to integrate RES. A microgrid uses DGs based on the local RES to support local loads with the support of energy storage systems (ESS) [5]. The system can also interface with the utility grid and export power to reduce the amount of conventional power plants.

Until recent years, most research and practical implementations focused on the

microgrids in AC distribution systems. As shown in Figure 1-1, a simple AC microgrid (ACMG) contains a PV source, a wind turbine generator, an AC load, a battery and a point of connection (POC) to the utility grid. Although the technology is now relatively mature and reliable, ACMGs have several disadvantages. Since PV sources and batteries operate in DC, voltage source converters (VSCs) are required to connect PVs and batteries to the AC bus [6]. In many cases, two-stage conversion is needed, which involves two converters. Meanwhile, transformers cannot link AC busses with different frequencies. ACMGs need complicated source conversion stages to connect the bus to wind turbine generators [7]. There is a significant power loss during the power conversion process [8][9]. To reduce the conversion stages and minimize power losses, DC microgrids are being promoted.

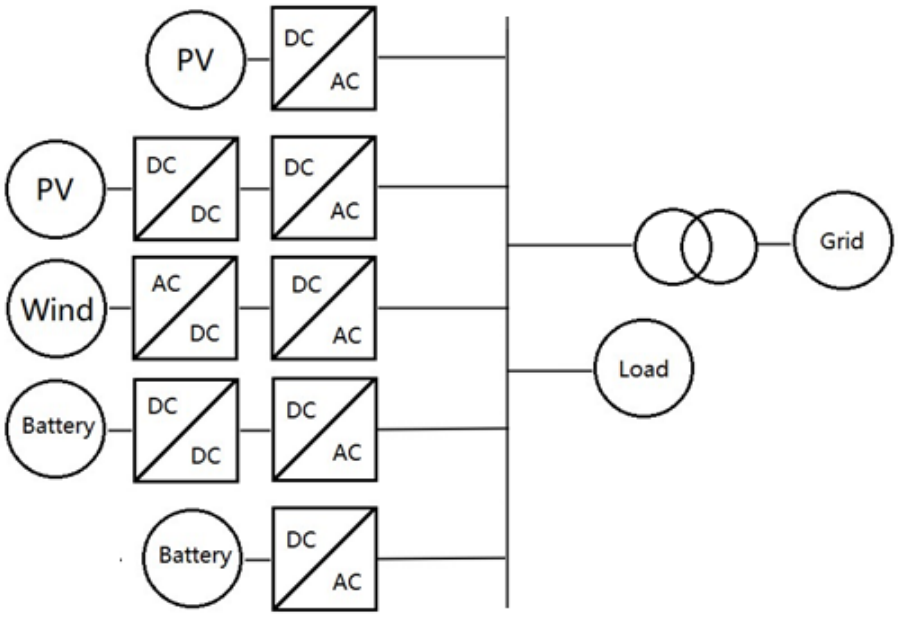

Figure 1-1: AC microgrid structure.

1.2 DC Microgrids

With the recent technological advances in semiconductors and power electronics, there is renewed interest in DC distribution systems. Although there has been an increasing number of high voltage DC (HVDC) transmission projects around the world [10], low voltage DC (LVDC) distribution has been restricted to few specific applications. LVDC distribution is an emerging concept, and DC microgrids (DCMGs) are typical LVDC power systems [11].

In Figure 1-2, the structure of a simple DCMG system is illustrated. The power conversion stages are reduced. The VSCs between the power generation and storage modules and the AC bus are eliminated. DCMGs use only DC-to-DC (DC/DC) converters, which have simpler structures and higher power efficiency, for PVs, batteries, DC loads and any other devices operating in DC power [12]. Meanwhile, most electronic loads such as laptops, televisions, microwave ovens, LED bulbs, etc. operate using DC power. Such DC loads require a rectifier (or VSC operating as a rectifier) to be connected to the AC system. However, in DCMGs, power efficiency can be improved by using DC/DC converters for those local loads [12]-[15]. Moreover, in DCMGs, reactive power compensation, frequency stability and synchronization problems are eliminated [12]. As a result, DCMGs have much easier topologies and control system architectures. Additionally, DC transmission can further improve the efficiency over AC transmission lowering the costs and power losses due to line skin effect [12][16].

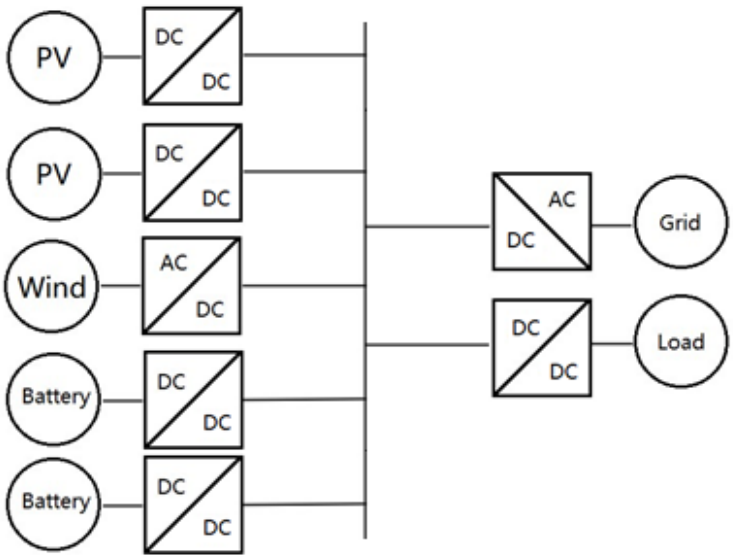

Figure 1-2: DC microgrid structure.

Owing to the above advantages, DCMGs have been gradually attracting the attention of electrical engineers. However, as research and simulation studies explore this option in depth, challenges and constraints have appeared. It has been proved that protection of DC distribution systems is much more difficult than AC systems [12][15][17]. Especially for DCMGs, standard protection methods or standards have not even formed yet.

In AC systems, protection technologies and devices have been mostly well established. However, in DCMGs, fault detection schemes and fault clearing methods are still under development, and researchers and development engineers are facing many challenges. In [17], several DCMG fault detection methods are discussed. These include overcurrent protection, current derivative protection, directional protection, distance protection and unit protection. In DCMGs, filtering capacitors will discharge immediately after the fault and contribute to the fault current, raising the magnitude of the fault current

in some cases over a hundred times of the nominal current, within a few milliseconds [17]. Therefore, fast speed of protection operation is a key feature in the DCMG protection [18]. It requires relays to accurately detect and discriminate a fault as soon as possible and trip the relevant DC circuit breakers (DC CBs) removing the faulted network section in millisecond time scale.

There are two main design requirements to be considered: speed and selectivity. The DCMG protection system must operate extremely fast, while it must also accurately determine the faulted area to minimize the extent of interruptions. The different fault detection methods must be considered with respect to these two aspects.

- Overcurrent Protection: The relay will send the tripping signal when it detects a current over the threshold value. However, due to signal transmission time and DC CB operation time, fault currents will keep increasing and can reach very dangerous levels. On the other hand, determining appropriate current thresholds that facilitate discriminating the faulty section is very difficult. This method does not satisfy the protection speed and selectivity requirements.

- Current Derivative Protection: The relay calculates the current derivative by comparing two consecutive current samples. As a result, current trend is predicted. The relay will trip the line when it detects a sudden rise in the derivative. This method can be fast enough. However, it is hard to set the pick-up value which depends on the line impedance, length of the lines and the fault resistance. Setting

thresholds to achieve the selectivity property is a considerable challenge. For example, consider the system shown in Figure 1-3. A high resistance fault (HRF) close to a relay can be confused with a low resistance fault (LRF) far away from the relay, as both these cases can produce similar rate of change of current.

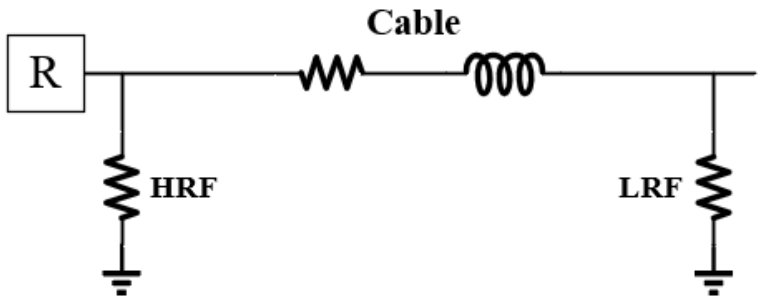

Figure 1-3: Current derivative method selectivity problem.

- Directional Protection: Regardless of the protection speed, there is a key issue when building the protection for DCMGs. Since in ring bus systems and meshed systems, normal and fault currents do not always flow in one direction due to generation variations of DGs or load changes. Directional protection can greatly support fault discrimination in these systems. Even in radial systems, the directional protection needs to be applied at battery and the grid point of connection (POC). The protection selectivity in a complex DCMG system is hard to achieve without directional protection. However, developing robust protection algorithms that can very fast detect the direction of fault current is a challenge.

- Distance Protection: This method calculates the resistance from the ratio of local

voltage and current. Regardless of the speed, selectivity is a challenge for distance protection. As discussed above in current derivative part, HRF detection is the main problem.

- Unit Protection: This method compares currents at all circuit branches connected the protection zone and tests whether the Kirchhoff's Current Law (KCL) is satisfied. The selectivity can be easily guaranteed. However, as communication links are required when employed for line protection, the unit protection needs additional time to make the decision. The communication delay makes the protection speed unsatisfactory. Moreover, in DCMG protection, sampling rate is very high. Correct data synchronization among relays is also a challenge.

Not only the fault detection of DCMG protection needs to be carefully designed, the fault current breaking device is also a big issue. In AC protection, circuit breakers (CBs) interrupt the fault current at natural zero crossing point in the waveform. However, this is not applicable in DC protection [12][18]. Since DC fault currents have no zero crossing points, ACCBs cannot be used for DC current interruption. New circuit breaker technologies applicable for the DC system is desired.

1.3 Research Objectives

The objective of this research is to develop a reliable DCMG line protection system satisfying the speed and selectivity properties discussed in the previous section. To

facilitate simulation studies, developing a DCMG test model is the first task. Then, DCMG fault analysis can be performed using the simulation model. Based on the understanding acquired, fault detection and localization methods can be designed for this model. The computer software PSCAD is used to simulate the DCMG model as well as the protection system. The main research goal is achieved through fulfilling the following sub-objectives:

- Literature review on DCMG configurations and operating modes.
- Implementation of a ring bus DCMG model on PSCAD software, including a simple energy management system.
- Introduction to DCMG grounding methods and protective devices (PDs).
- Analysis of the fault current properties and design of protection methods.
- Evaluation of the proposed protection schemes with respect to the design objectives.

1.4 Research Contributions

The contributions of the research include a detailed simulation model of a ring bus DCMG in PSCAD, simplified analytical expressions for calculating initial fault currents due to faults in a ring bus DCMG which are shown to be fairly accurate through detailed simulations, and establishment of different protection requirements for low and high resistance faults are demonstrated. Two main contributions of this research are the local current derivative based low resistance fault detection and discrimination method and the

local to remote end current derivative ratio based high resistance fault detection and discrimination method. It was also shown that the protection settings can be easily computed from the approximate analytical expressions for the initial rate of change of currents. A complete protection scheme is developed combining the two concepts. The contributions also include a method to determine the location of a fault based on the double ended protection algorithm.

1.5 Thesis Organization

This thesis has seven chapters. The first chapter is the introduction.

Chapter 2 reviews the relevant literature and illustrates the implementation of a ring bus DCMG model in PSCAD. This includes power electronic converters interfacing a PV source, the AC grid, DC loads and an ESS with the DC bus. Different operating modes and their corresponding control systems are also shown.

Chapter 3 discusses DCMG fault types and properties. The impact of the grounding method is analyzed. The natural response of the DCMG fault is analyzed, and based on this, protection design objectives are made.

Chapter 4 develops a current derivative protection method based on local measurements. In this method, LRFs are detected within two protection requirements.

Chapter 5 develops a unit protection method based on the current derivative ratios. In this method, HRFs are well detected and eliminated.

Chapter 6 discusses the fault location calculation method. It uses the current derivative ratios from the Chapter 5 and accurately calculates the fault location on the faulted cable.

Chapter 7 concludes the research and the whole protection scheme and suggests some future works.

Chapter 2 DC Microgrid Model Implementation

2.1 DC Microgrid Configurations and Operating Modes

In this section, different possible configurations of a DCMG are introduced and various operating modes are discussed briefly.

2.1.1 DC Microgrid Configurations

A DCMG is a low voltage DC power system in a local area. It generates electric power to satisfy the local demand. A typical DCMG usually contains distributed generation, energy storage elements such as batteries, loads and a point of connection to the utility grid. Each device connects to a common DC bus through a power electronic converter. For devices like PV arrays, batteries and DC loads which operate with a DC voltage, DC/DC converters are used; for the elements such as wind turbine generators and the utility grid which work with AC voltage, VSCs are used in the connection to the DC bus. In case of power unbalance due to non-deterministic generation such as PV and wind turbines, power flow is well maintained by the energy storage system (ESS) or the utility grid depending on the DCMG operating mode [19][20][21].

Differing from the utility grid that has long transmission length and complicated structure, microgrids only cover small areas, and their structures are much simpler. There

are normally three types of structures for DCMGs [5][22], as shown in Figure 2-1: the radial structure shown in Figure 2-1(a), the ring structure shown in Figure 2-1(b), and the meshed structure Figure 2-1(c).

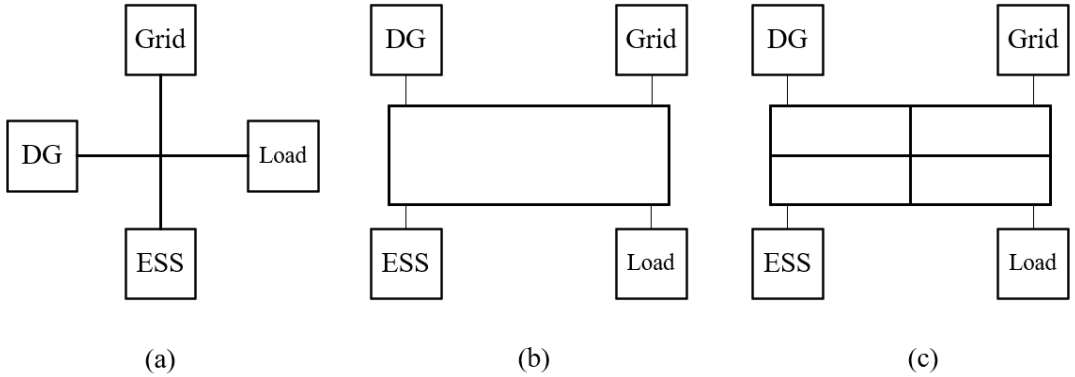

Figure 2-1: DCMG structures (a) radial, (b) ring, and (c) meshed structures.

- Radial Structure: This system has the simplest configuration. However, the radial structure is of poor reliability [5]. If a fault happens on a line, the device at the end of the faulted line is completely out of the power. This situation can potentially cause the collapse of the whole system due to the power flow unbalance.
- Ring Structure: This structure is preferred by many researchers. Compared to the meshed system, this configuration is much simpler. An element connected to a ring bus system has two alternative transmission paths. This guarantees that the system does not lose any devices under a single line fault [23][24]. However, since current can flow through both paths in either direction, protection coordination becomes difficult [17].

- Meshed Structure: This structure has the highest reliability [25]. It can sustain multiple faults without collapse. However, protection design and setting are extremely complicated for a meshed system [26].

In this research, a ring structure DCMG is established. Since only single line fault is analyzed, a ring structure system is enough to simulate and infer a transmission line protection method which is also suitable for a meshed system and at the same time, reduce the model complexity to improve the research efficiency.

2.1.2 DC Microgrid Operating Modes

In a DCMG, the local devices only contain DGs, batteries and loads. The utility grid is an external component that in many cases needs a long transmission line to be connected to the DCMG. Since this external part is not always switched on for the DCMG, the system works differently with the connection status of the grid. Based on this concept, there are two different operating modes [12].

The first mode is the grid-connected mode. In this mode, the utility grid is switched on for the DCMG. The excess generation in the DCMG can be exported to the utility grid without generation curtailments. When there is a power deficit in the DCMG, the grid can also work as a supplementary source. To avoid conflict between the grid and the battery, in the grid-connected mode, the battery is either turned off or slowly charged by a constant power. Therefore, voltage regulation and power balance are performed by the utility grid

[20][27], as shown in:

$$P_{grid} = P_{DG} - P_{load} - P_{battery} - P_{loss}. \quad (2\text{-}1)$$

The power difference between the sources and sinks is maintained by the grid. In this situation, the DGs are the sources. The battery, DC loads, transmission loss and switching loss are the sinks.

The second mode is the islanded mode. Since the utility grid is switched off, the battery becomes the only device that can maintain the system power balance. Therefore, the bus voltage and power balance are controlled by the battery [28], as expressed in (2-2):

$$P_{battery} = P_{DG} - P_{load} - P_{loss}. \quad (2\text{-}2)$$

In the islanded mode, the battery is not always a sink anymore. During a power surplus, the battery maintains the power flow by charging the extra power. During a power shortage, it discharges to support the DGs. With the knowledge of the configurations and operations of DCMGs, a DCMG model for the research study is established in the next section.

2.2 DC Microgrid Model Design

Details of the DCMG developed for studies in this thesis are briefly described in the next few sections.

2.2.1 Basic Structure

In this research, a ring bus DCMG is considered and a model of it is built in PSCAD electromagnetic transient (EMT) simulation software. This model has five elements:

- PV System: This element contains a PV array and a DC/DC boost converter connecting to the DC bus. The switching circuit is controlled by an MPPT controller to ensure largest possible power generation under a given radiation level and cell temperature.
- Grid Connection: This element contains an AC grid and a bi-directional VSC connecting to the DC bus. The VSC control system is designed in d-q reference frame. In the grid-connected mode, this element maintains the power flow and the bus voltage.
- Energy Storage System: This element contains a battery bank, a bi-directional DC/DC converter and a battery management system (BMS). In the grid-connected mode, the batteries will be slowly and continuously charged when the state of charge (SOC) of the batteries is low or discharged if the SOC is high and high RES generation is expected in the next few hours. In the islanded mode, ESS maintains the power flow and the bus voltage.
- Two DC Loads: A constant resistive load and a DC/DC buck converter in constant output voltage mode is in each load element.

The topology of this ring bus DCMG is shown in Figure 2-2.

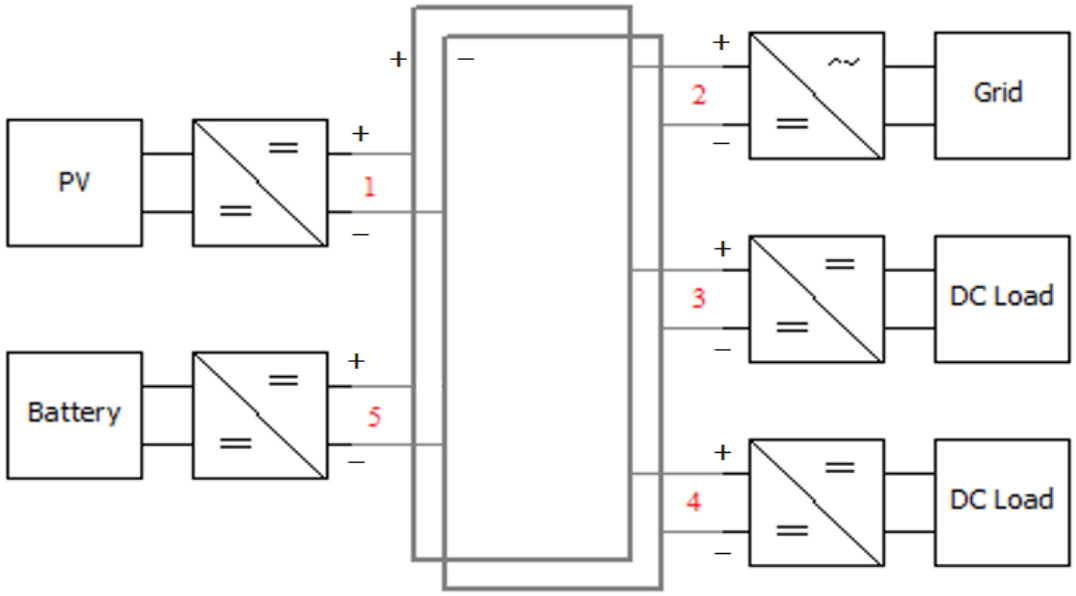

Figure 2-2: Ring bus DCMG topology.

The nominal voltage of the DCMG is 400 V (±200 V). The 400 V DC ring bus is connecting with the five elements mentioned above. The PV system is connected at Bus-1 with 200 kW maximum power generation. Depending on the solar irradiation and panel temperature, the power can vary from 0 to 200 kW. The grid connection is at Bus-2, and the AC grid is simulated as an infinite bus. Two fixed DC load elements are connected at Bus-3 and Bus-4, and their nominal power demands are both 100 kW. The ESS is at Bus-5. Its maximum charge/discharge power is 200 kW. Each cable between two busses is 100 m long. Since filtering capacitances are large, the cable is simulated as a series RL circuit.

The design parameters are shown in Table 2-1.

Table 2-1: Design Parameters

Parameter	Value
DC Bus Voltage	400 V (±200 V)
PV Power Supply	200 kW
Fixed DC Load	100 kW
Load Voltage	48 V
Battery	200 V, 200 kW
Cable Length (all cables)	100 m
Cable Resistance and Inductance	70 mΩ/km, 300 μH/km
Filtering Capacitance	10 mF

2.2.2 Photovoltaic Source

The PV source is connecting to the DC bus through a DC/DC boost converter as shown in Figure 2-3. The DC/DC boost converter steps up the PV output voltage to the 400 V DC bus voltage. Two power switches are controlled by a MPPT controller, a PI controller and a PWM controller. The MPPT controller receives the output voltage and current from the PV source and using “Perturb and Observe” method to find the maximum

power point PV operating voltage and current [29].

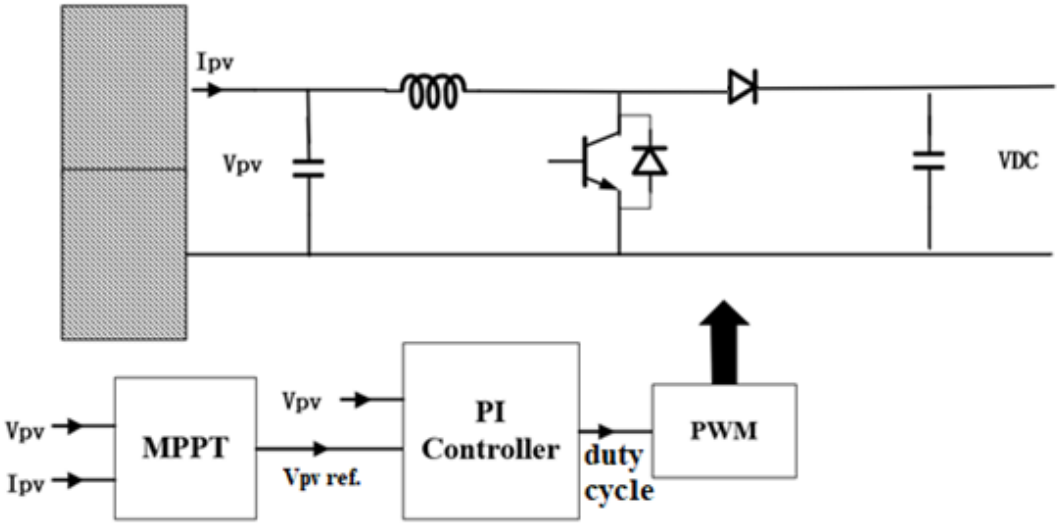

Figure 2-3: PV source.

2.2.3 Utility Grid Connection

The AC infinite bus is connecting to the DC bus through a transformer and a VSC. The topology of the bi-directional VSC is shown in Figure 2-4, and it is controlled by d-q controller [30]. In the grid-connected mode, the VSC regulates the DC bus voltage at 400V, and controls the reactive power to a specified reference value, which is usually set at zero. This converter will ensure the power balance in the DCMG system. When there is a power surplus, the VSC operates as an inverter to upload power to the grid. When there is a power shortage, the VSC operates in rectifier mode and supplies power to the DC side.

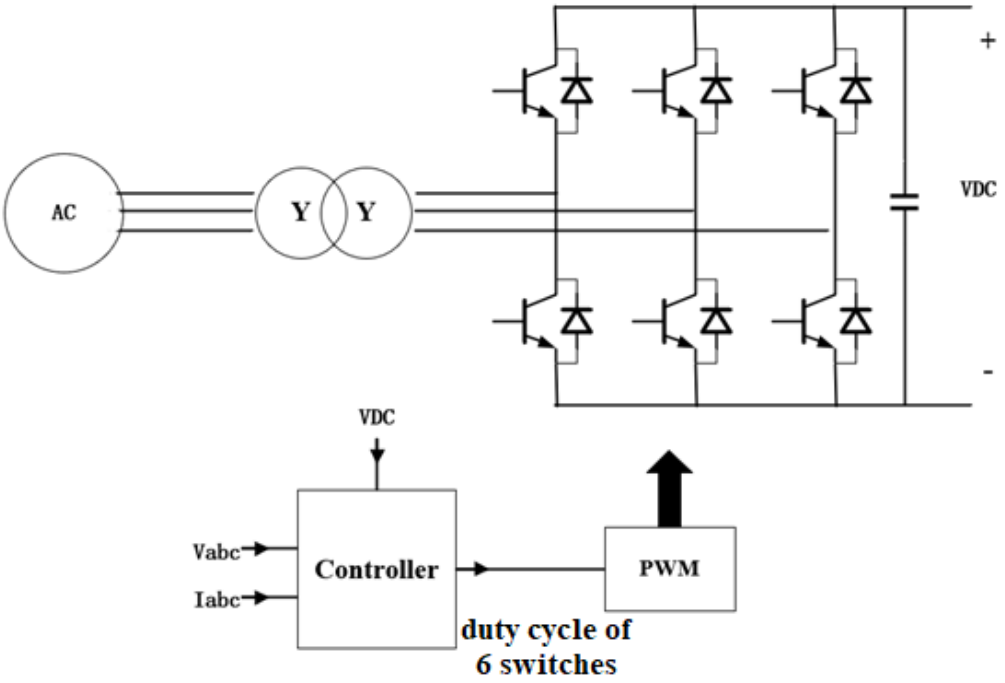

Figure 2-4: Utility grid connection.

2.2.4 DC Loads

The two DC load elements have the same configuration and control system. The DC/DC buck converter steps down from the bus voltage 400V to the load voltage 48V. A double loop control system consisting of outer voltage loop and inner current loop is applied to them as shown in Figure 2-5.

2.2.5 Energy Storage System

In the ESS, a bi-directional DC/DC converter is linking a battery bank and the DC bus. The control system of the ESS is complicated. There are two operating mode in DCMGs. The battery will work differently in the two modes.

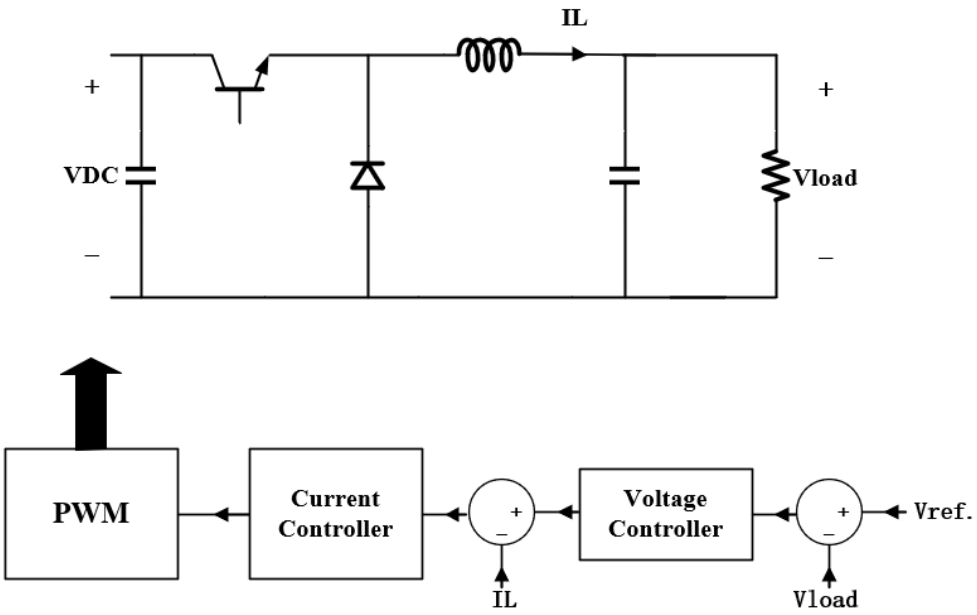

Figure 2-5: DC load.

In the grid-connected mode, the utility grid maintains the bus voltage. In this scenario, the battery will be continuously charged until it is charged to a maximum SOC value [31]. This is called the constant power charging mode, and the battery is charged at 20kW. The DC/DC converter works as a buck converter stepping down the voltage. Although more sophisticated charging control may be required depending on the battery type, only constant power charging is implemented as it is sufficient for intended protection studies.

In the islanded mode, the utility grid is disconnected. Then, the ESS must control the bus voltage. This is called the constant voltage mode. In this case, the ESS maintains the power balance [20][21][31]. When a power shortage happens, the battery is in discharging mode to provide additional power to the DC bus; when the generated power is greater than the sum of the load and the power loss, the battery is in charging mode to sink any

power surplus [28].

The above control method is the battery management system (BMS). The BMS is the most important control system in this model to guarantee the normal operation of the DCMG in both operating modes under transient period and steady state period. In Figure 2-6, the constant power mode controller is illustrated, and in Figure 2-7, the constant voltage mode controller is illustrated.

In power system protection, faults develop in very short periods. In this research, fault detection and clearance are considered in the system normal conditions (no generation curtailment and load shedding), and the BMS only considers battery state of charge (SOC) in the normal range, between 40% and 90%.

2.2.6 Change of Modes

When switching between the grid-connected mode and the islanded mode, there exists a transient response. In the fault detection design, the protection system must ignore the current oscillation caused by the transient response. Since this research focuses on the current derivative based protection, line current derivatives are inspected by relays. To reduce the rate of change of the current during the change of mode transient period, the utility grid is connected to/disconnected from the system by closing/opening the CBs at the AC side using the zero crossing property to gradually reduce the current value. Hard current interruption at the DC side will cause significantly large current derivative that

results in mal-functions of the relays.

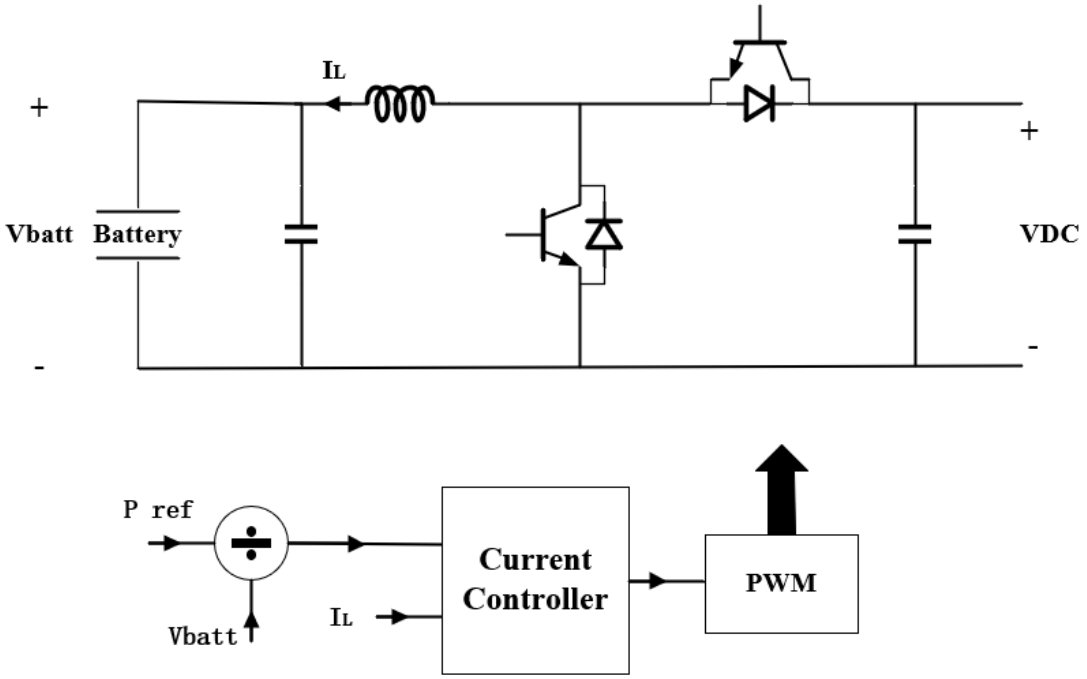

Figure 2-6: Battery in constant power mode.

2.3 Simulation Results

The DCMG model shown in Figure 2-2 is built in PSCAD. All converters use 20 kHz as switching frequency for generating PWM signals. The simulation time step is 10μs.

Simulations were performed to prove the stability and reliability of the model. In this research, transient responses in the grid-connected mode and the islanded mode were simulated. The change of mode test was also performed.

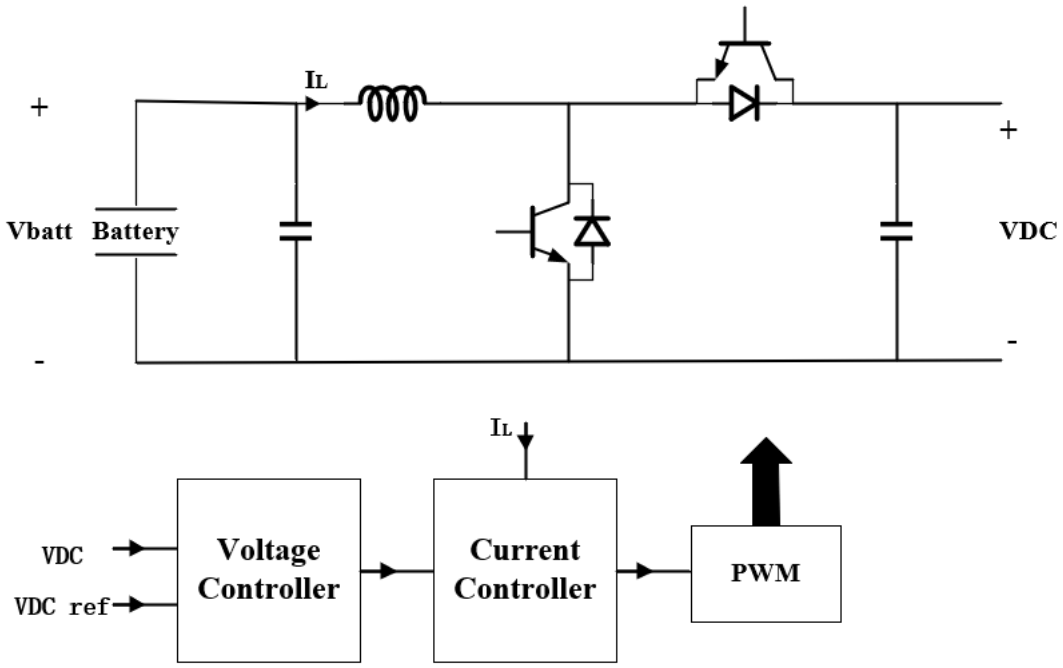

Figure 2-7: Battery in constant voltage mode.

2.3.1 The Grid-connected Mode Operation

In the grid-connected mode, initially the system steady state performance was checked. Then, change of PV supply was done to test the stability of the whole system when the power balance is maintained by the grid VSC.

In this case, the solar irradiance and the temperature of the PV source were initially set at 800 W/m^2 and 25 ^{o}C, resulting in 200 kW of power injection from the PV source. The ESS was in the constant power mode and charged at 20 kW. Each DC load was consuming 100 kW power. The system operated in steady state until simulating time is 2.0 s as shown in Figure 2-8. A positive power means a source, and a negative power means a sink in the DCMG system.

At time 2.0 s, the solar irradiance was decreased to 500 W/m^2, the transient response is shown. As the PV generation decreases, the utility grid sends more power to the DCMG. The DC bus voltage remained stable. When the time is 3.0 s, the solar irradiance was increased back to 800 W/m^2. It can be seen from the graph that the grid reduces power to the DCMG, and the bus voltage is still regulated at 400 V.

2.3.2 The Islanded Mode Operation

In this mode, a similar test was performed to the model. Since the grid was switched off, the ESS was in the constant voltage mode. The PV generation reduction happened at 1.0 s and recovered at 1.6 s. The result is shown in Figure 2-9. With the power compensated by the battery, the system is well controlled: the power balance maintained, and the bus voltage is regulated at 400 V.

2.3.3 Change of Mode of Operation

In this case, the model was tested for changing of operating mode. Initially, the DCMG model was in the grid-connected mode. At time 1.11 s, it was changed to the islanded mode, and at 1.6 s, it was changed back to the grid-connected mode. From the simulation result in Figure 2-10, it can be seen that the system was well regulated.

From the above three tests, the system operation is proved to be stable and reliable. Each element was working properly. The bus voltage and power balance were well maintained by the control system in both operating modes.

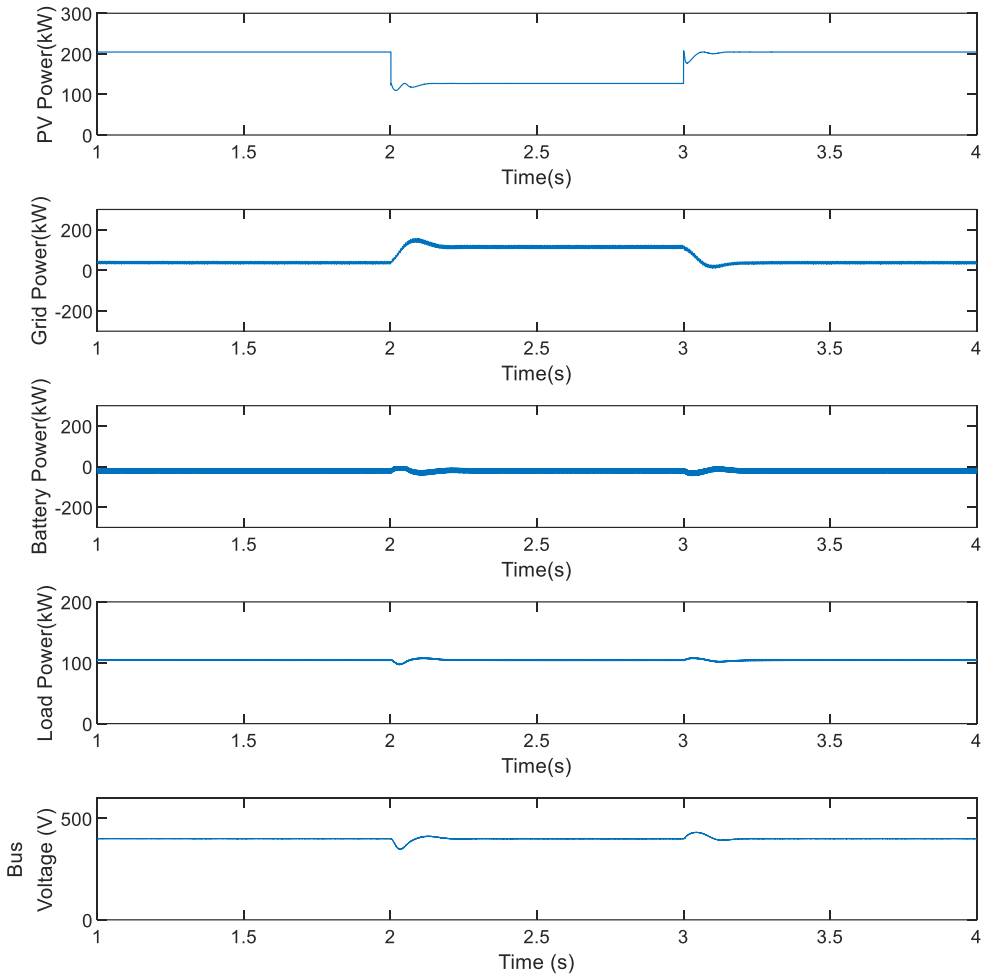

Figure 2-8: Grid-connected mode simulation result.

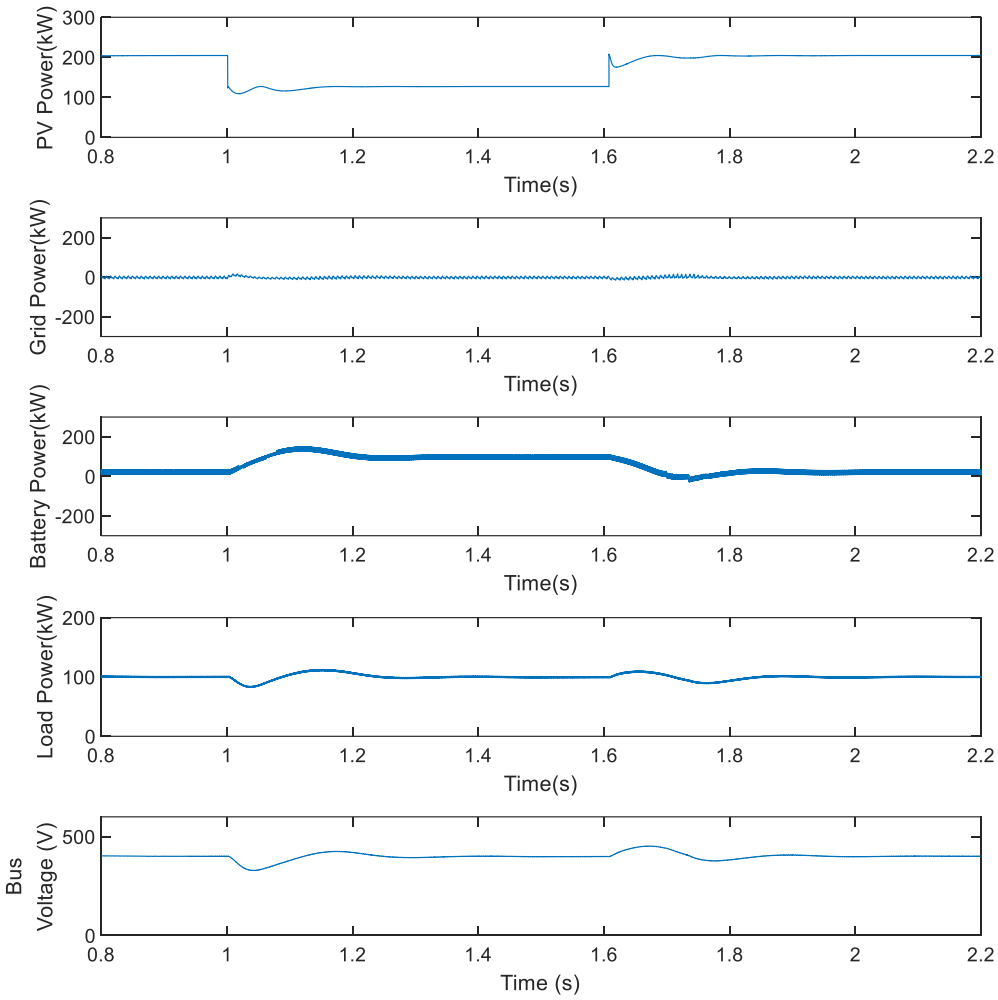

Figure 2-9: Islanded mode simulation results.

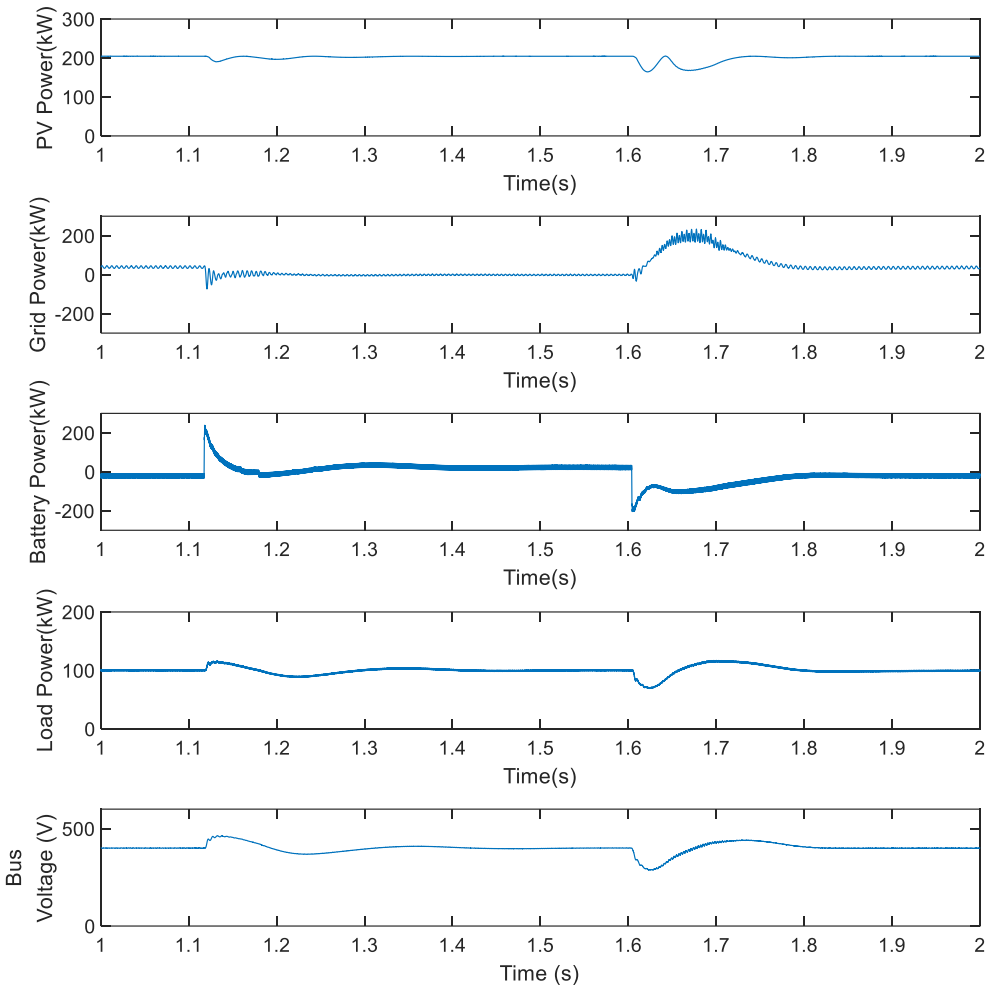

Figure 2-10: Change of mode simulation results.

2.4 Summary

This Chapter specifically discusses the implementation of a ring bus DCMG model consisting of a PV source controlled by a MPPT controller, a battery, two loads and an interface to the AC grid. The battery and its BMS control scheme are presented. The model is designed to operate in the grid-connected and the islanded mode. In these two different modes, the system stability is ensured by the implemented control methods. The utility grid regulates the DC bus voltage in grid-connected mode, and the ESS regulates the DC bus voltage in the islanded mode. The shift of the control schemes between two modes is handled by the BMS. From the simulation results, it can be seen that the implemented DCMG model is robust.

The steady state operation of the DCMG model is confirmed and the next step before protection design is understanding the characteristics of the fault currents. Therefore, before establishing the protection scheme, DCMG faults should be analyzed. Moreover, some protective components are necessary to be added to the simulation model. These includes grounding circuits and the DC CBs. A specific discussion including the above information will be provided in the next chapter.

Chapter 3 DC Microgrid Protection Design Requirements and Fault Analysis

3.1 Introduction

DCMG is an emerging concept and currently, there is no standard protection method that is widely accepted by the industry [32]. Although designing the detection and localization methods for DCMGs involves a lot of challenges, some basic theories and requirements have been defined.

Firstly, in a floating DCMG system, it is not possible to detect the first pole-to-ground fault [33], causing a risk for a second pole-to-ground fault before detecting the first fault. Also, it is difficult to define the rating of the insulation in an ungrounded DCMG [34]. Therefore, an appropriate grounding method must be applied to any practical DCMGs.

To develop a fault detection and localization system, the DCMG fault response must be analyzed. As discussed in this chapter, a DCMG fault will cause the currents to quickly rise to several tens of the nominal current magnitude; in critical cases, over a hundred times. Due to this feature, faults must be tripped fast. When the fault response is defined, protection design becomes possible.

Furthermore, it has been clearly proved that an AC CB is not suitable to clear a DC fault due to non-exist of the natural zero crossing point in DC currents [12][18]. Therefore, a suitable DC CB for DCMG faults is essential.

Therefore, this chapter will show some definitions of the DCMG protection devices and the fault response. These definitions will be used throughout the rest of the thesis as the protection design criteria.

3.2 DC Fault Types

In a DC distribution system, there are mostly two types of DC faults [15][16][18][34]. In Figure 3-1 (a), a fault linking the positive pole and the negative pole of the DC line is shown. This type of DC faults is called a pole-to-pole (PP) fault. In Figure 3-1 (b) and (c), a fault linking either poles to the ground is called a pole-to-ground (PG) fault. A third type of fault, a pole-to-pole-to-ground fault is possible but is rare. Also, the characteristics of pole-to-pole-to-ground faults are similar to that of pole-to-pole faults. Therefore, this type of faults is not discussed separately.

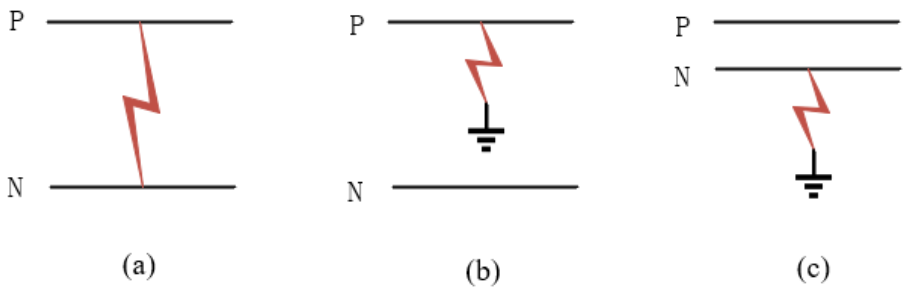

Figure 3-1: DC faults (a) pole-pole (b) positive pole-ground (c) negative pole-ground.

A DC PP fault connecting two poles usually involves a low fault resistance [18]. As a result, a large fault current is generated. Detection of a PP fault is easier, since it is not

relevant to grounding methods. However, a PG fault is different. Detection of a PG fault highly depends on the grounding method of the system. According to [35], PG faults happens more frequently than PP faults. Therefore, an appropriate grounding method is chosen in the next section. Furthermore, since a PG fault often involves a high fault resistance, detection of a PG fault is much harder.

These two types of DC faults will be simulated in this research. The main design objective is to detect and clear these faults within the protection requirements.

3.3 DC Microgrids Grounding Methods

Since this research is based on computer simulations, the grounding methods discussed in this section will only consider the circuit topology without any realistic parts like the device metallic surface. In terms of circuit topology, there are three grounding methods proposed in literature for DCMGs.

3.3.1 Ungrounded DCMGs

The first method is leaving the system ungrounded. Ungrounded systems have the lowest cost and the simplest system configuration [36]. This method can be used for low power systems [37]. However, for a large DC power system, the system must be grounded for two reasons [34]:

- Insulation: An ungrounded floating system has no voltage reference level. Therefore, insulation rating cannot be decided. Once a PG fault happens, the unfaulted line has

a risk voltage value with respect to the ground.

- Second PG fault: an ungrounded system cannot detect the first PG fault. However, a second fault on the opposite line will cause huge risks as these two faults are equivalent to a PP fault.

Due to these two reasons, the ungrounded method is not applicable for the DCMG model in this research.

3.3.2 Negative Pole Grounding

The negative pole grounding method, as shown in Figure 3-2, defines a voltage reference point for the DCMG system with simple configuration. As a result, the system is not floating anymore. The positive pole has the same voltage as the DC bus voltage, which is 400V. Therefore, the insulation rating can be defined.

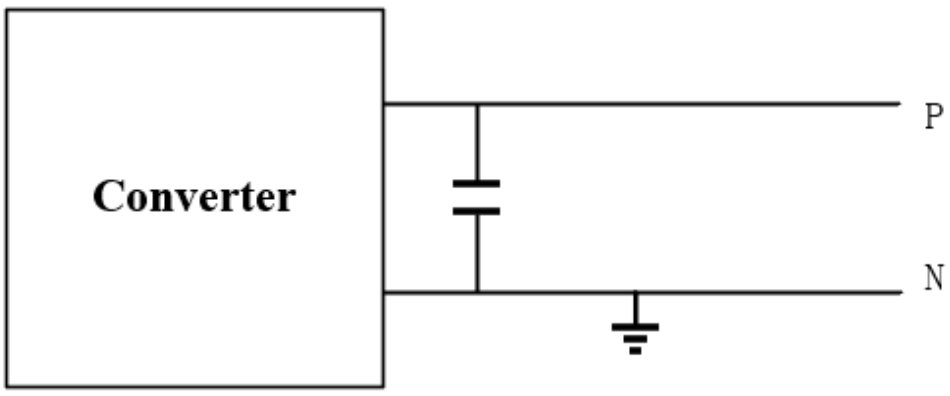

Figure 3-2: Negative pole grounding topology.

However, this method is equivalent to an ungrounded system with a low resistance PG fault on its negative pole. Therefore, the system has a risk when a PG fault on the positive pole happens, turning the PG fault into a PP short circuit [38].

3.3.3 Middle Point Grounding

The middle point grounding method has been the preferred grounding method for most of the DCMG systems discussed in literature. As shown in Figure 3-3, two series capacitors replace the filtering capacitor, and the middle point is solidly grounded.

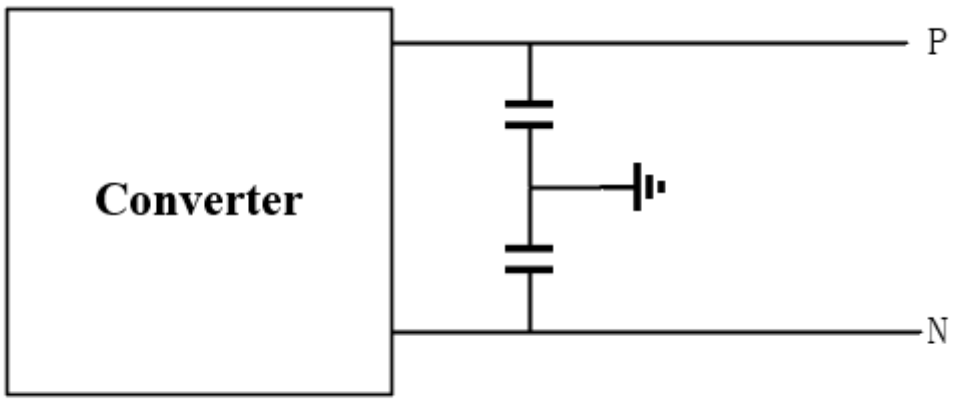

Figure 3-3: Middle point grounding topology.

Compared to previous two methods, the middle point grounding method has a complicated grounding topology which has the highest cost. However, there are many advantages. First of all, it decreases the insulation ratings [5][34][38]. Since the middle point of two capacitors with the same capacitance is solidly grounded, the voltage rating on the two poles are ± 200 V. The cost of the insulation system is reduced from the 400

V rating. Moreover, with the grounding capacitor in between, a PG fault on either pole is not going to create a direct PP short circuit problem anymore, improving the reliability of the whole system.

Despite with these benefits, there is still a risk for the middle point grounding method. When a PG fault happens, the faulted line is in 0 V rating. With the continuous maintenance of the DC bus voltage, the voltage rating of the unfaulted line becomes 400 V instead of 200 V, causing an overvoltage stress. Therefore, when middle point grounding method is used, a PG fault must be cleared fast. After comparing the pros and cons of all three grounding methods, the middle point grounding method is suggested for the DCMG considered in this research.

3.3.4 Transformer Secondary Side Configuration

At the grid connection, the AC bus is connecting to the VSC through a step down three-phase transformer. If the secondary side (VSC side) is Y-connected with the neutral point grounded, it can provide a returning path for a DCMG PG fault [39]. As shown in Figure 3-4, when a positive PG fault is applied to the DCMG model, the fault current generated from the transformer flows into the fault path and flows back from the neutral point. To overcome this problem, the transformer's secondary side must leave ungrounded or use delta-connection.

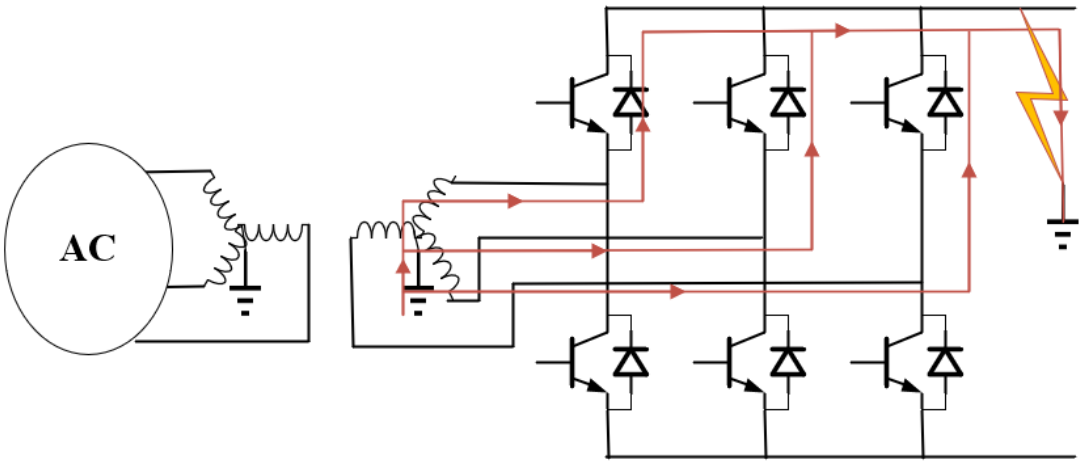

Figure 3-4: Transformer grounding problem.

3.4 DC Microgrid Fault Analysis

Using the middle point grounding method at all elements, the bus side of each converter, either AC/DC or DC/DC, has the consistent grounding capacitors topology. These grounding capacitors can contribute a significant amount of the fault current during a fault. This is explained in the following.

In DCMGs, different types of faults can cause different fault current response. However, there is a common phenomenon at their initial periods. According to [17][40][41], the initial fault response under either a PP fault or a PG fault is an RLC response. As shown in Figure 3-5, the equivalent circuit of the initial fault response contains only a resistor, an inductor and a capacitor. The R stands for the sum of the fault resistance and the cable resistance. The L is the cable inductance. The C is the grounding capacitance.

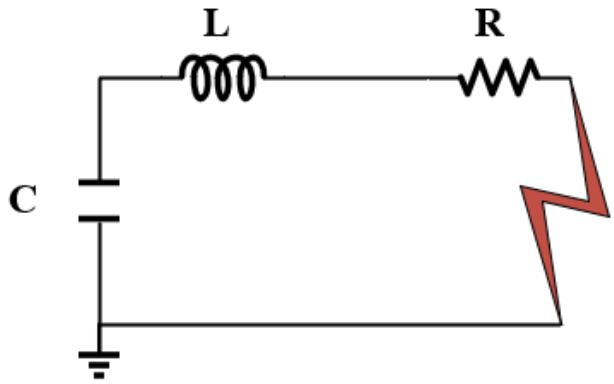

Figure 3-5: Initial fault response.

Applying Laplace transformation, the analytic function of the RLC response is as:

$$I(s) = \frac{\frac{V(0)}{L} + I(0)s}{s^2 + \frac{R}{L}s + \frac{1}{LC}} \tag{3-1}$$

where V(0) and I(0) are the initial voltage across the grounding capacitor and the initial current through the cable inductor. From (3-1), a time domain equation of the fault current using inverse Laplace transformation is expressed as:

$$i(t) = \frac{V(0)}{L(s_1 - s_2)}(e^{s_1 t} - e^{s_2 t}) + \frac{I(0)}{(s_1 - s_2)}(-s_1 e^{s_1 t} + s_2 e^{s_2 t}) \tag{3-2}$$

where s_1 and s_2 are two poles of (3-1) which are equal to:

$$s_1, s_2 = -\alpha \pm \sqrt{\alpha^2 - {\omega_0}^2}. \tag{3-3}$$

The damping factor α and the resonance frequency ω_0 in (3-3) are:

$$\alpha = \frac{R}{2L} \tag{3-4}$$

$$\omega_0 = \frac{1}{\sqrt{LC}}. \quad (3\text{-}5)$$

In DCMGs, during the initial RLC response, the V(0) term of the fault current equation (3-2) is the dominant term [40], because the fault current is mostly contributed by the capacitor. Therefore, I(0) term is neglected. The fault current is approximated as:

$$i(t) = \frac{V(0)}{L(s_1 - s_2)}(e^{s_1 t} - e^{s_2 t}). \quad (3\text{-}6)$$

Comparing magnitudes of α^2 and ω_0^2 in (3-4) and (3-5), the fault current expression (3-6) can be classified as under-damped response and over-damped response. When $\alpha^2 < \omega_0^2$, the system is in under-damped response, which is expressed as:

$$i_{ud}(t) = \frac{V(0)}{L\sqrt{\omega_0^2 - \alpha^2}} e^{-\alpha t} \sin(\sqrt{\omega_0^2 - \alpha^2}\, t) \quad (3\text{-}7)$$

when $\alpha^2 > \omega_0^2$, the system becomes over-damped and the fault current is given as:

$$i_{od}(t) = \frac{V(0)}{L(s_1 - s_2)}(e^{s_1 t} - e^{s_2 t}). \quad (3\text{-}8)$$

To clearly observe the fault current initial response, a simulation was performed. As shown in Figure 3-6, a PP fault was simulated at time 0.3 s with a low fault resistance at 0.1 Ω. The grounding capacitance is 20 mF, and the faulted cable inductance is 10μH. From the simulation result in Figure 3-7, the initial RLC fault response is an extremely short period. It is also proven that the fault current in the initial period is mostly contributed by discharging grounding capacitors. The fault current from the source (DG, grid or battery) through the converter is negligible. During this short period, the fault

current has already reached a dangerous level comparing to 250 A nominal current. In the protection design, to detect an LRF is not hard. However, to detect and trip the LRF fast is one of the protection difficulties.

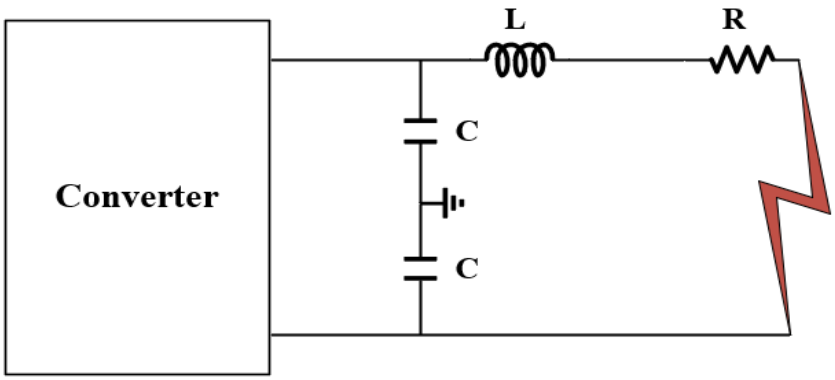

Figure 3-6: Fault response simulation.

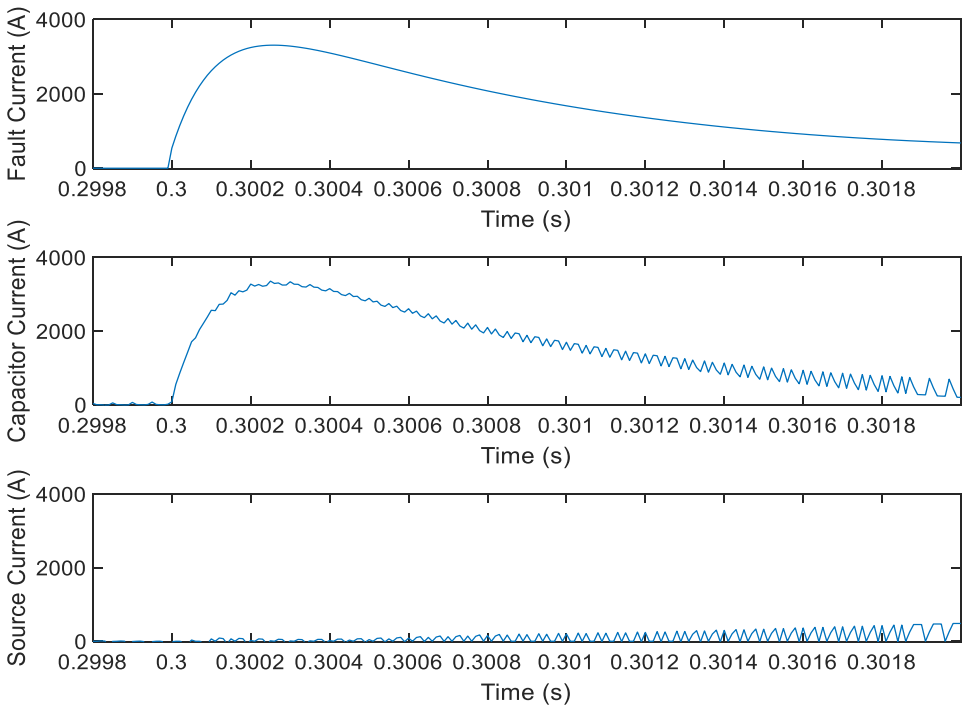

Figure 3-7: Initial fault response of an LRF.

Instead of an LRF, an HRF with 1 Ω fault resistance was simulated in the circuit shown in Figure 3-6. The result is shown in Figure 3-8. During the initial RLC response period, the fault current is mainly supplied by discharging capacitors, which is the same as an LRF response. The fault current in an HRF is not too large as an LRF, and the current increasing rate is slower. This causes challenges for the HRF detection. To accurately detect HRFs is another design objective considered in this thesis.

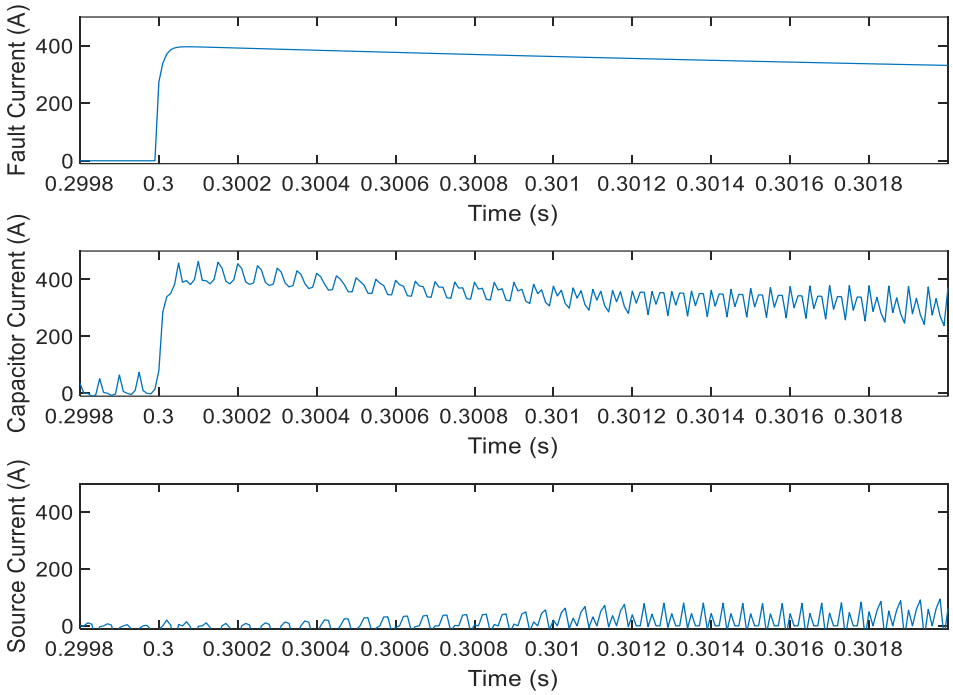

Figure 3-8: Initial fault response of an HRF.

From the two simulation results, the global peak of the DCMG fault current is from the initial fault response. Therefore, in this research, the protection objective is to eliminate the faulted part from the system during the initial fault period as fast as possible with good accuracy.

3.5 Solid-State Circuit Breaker

In the previous section, fault current responses were discussed. From Figure 3-7, the high fault current reaches its peak value within about 200 μs. In order to protect power electronic switches, the fault must be cleared in sub-millisecond time-scale. Moreover, normal AC CBs are not suitable for DC faults since there is no natural zero crossing point in DC currents. These constraints highlight the need for more capable DC CBs.

As discussed in [17][42]-[45], solid-state circuit breakers (SSCBs) are designed for clearing DCMG faults. A basic structure of an SSCB contains two pairs of inverse paralleled diode and a controllable switch, which are connected in series and in opposite directions, as shown in Figure 3-9. This type of CBs allows current flowing in both directions, and the hard DC current interruption is achieved by providing zero voltage signal at gates of both switches (IGBTs, MOSFETs or Thyristors). A normal switch is also connected in series to provide physical isolation. The operating time of SSCBs can vary up to 20 μs [42], which is ultrafast. Therefore, using SSCBs satisfies the DCMG fault clearance requirements of this research.

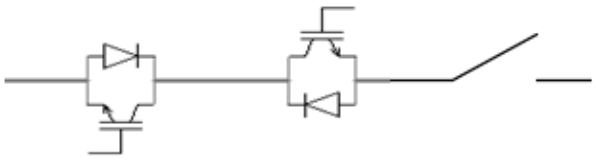

Figure 3-9: Solid-state circuit breaker topology.

In Figure 3-10, each cable of the DCMG model is protected by two protective devices

(PDs) at both ends. In each PD, there is an SSCB and a relay. The algorithm of the relay is discussed in later chapters.

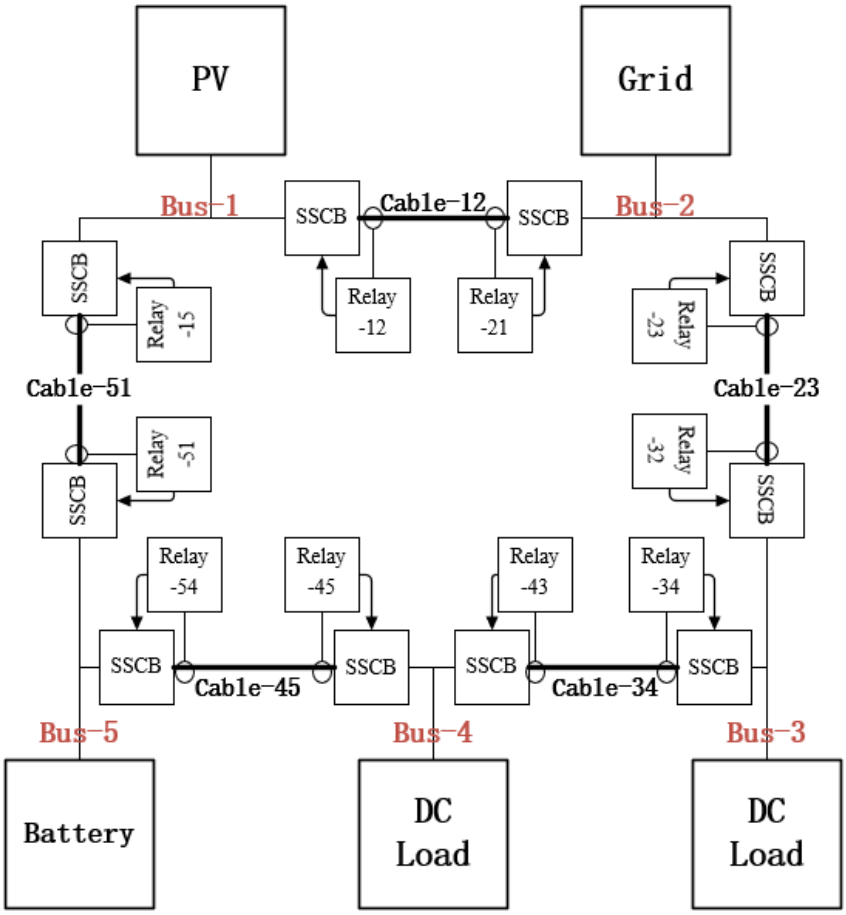

Figure 3-10: Arrangement of the protective devices of the ring bus DCMG.

3.6 Summary

This chapter has discussed some key definitions of the DCMG protection. The grounding method influences the fault current response, the insulation design and the fault detection algorithm. The middle point grounding method is selected for its low insulation rating and low risks for any types of faults. The common initial fault response is analyzed,

and analytical equations are derived considering a simplified equivalent circuit. The simulation results proved that the features of the DCMG fault currents are similar to the response of an RLC circuit. The analysis also highlights the protection speed requirement when designing a fault detection system in the next chapter of the thesis. Finally, an appropriate type of circuit breakers has also been chosen. Using SSCBs, the fault clearance speed is guaranteed.

Now, most important features of DCMG faults have been defined. With the knowledge in this chapter, based on the model built in Chapter 2, the protection scheme for a ring bus DCMG can be designed.

Chapter 4 Detection of Low Resistance Faults

4.1 Introduction

In DCMGs, low resistance faults (LRFs) are DC faults with low fault resistances, high current derivatives and extremely large fault currents. If not cleared immediately, large fault currents caused by LRFs will destroy power electronic devices and converters, resulting in the collapse of whole DCMG system. Therefore, the main design objective of DCMG protection is the fault detection speed.

As discussed in Chapter 1, the current derivative protection has the best fault detecting speed. It can predict the overcurrent issues earlier than the overcurrent protection, and not constrained by the communication delay compared to the unit protection. Therefore, in this chapter, a current derivative protection method with only local measurements is proposed to protect a ring bus DCMG.

4.2 Fault Current Derivatives

The time domain expressions in (3-7) and (3.8), which describe the variations of the fault currents immediately after a DC fault, were derived in Chapter 3. From (3-7), the current derivative of an under-damped system can be obtained as:

$$\frac{di_{ud}(t)}{dt} = \frac{-\alpha V(0)e^{-\alpha t}}{L\sqrt{\omega_0{}^2-\alpha^2}} \sin(\sqrt{\omega_0{}^2 - \alpha^2}t) + \frac{V(0)e^{-\alpha t}}{L} \cos(\sqrt{\omega_0{}^2 - \alpha^2}t). \qquad (4\text{-}1)$$

From (3-8), the current derivative of an over-damped system is derived as:

$$\frac{di_{od}(t)}{dt} = \frac{V(0)}{L(s_1 - s_2)}(s_1 e^{s_1 t} - s_2 e^{s_2 t}). \quad (4\text{-}2)$$

As per (4-1) and (4-2), the fault current derivatives attenuate with time as they both are functions with negative exponential terms. The fault current magnitude is also affected by the cable inductance: the further a fault is away from a relay, the smaller the measured derivative will be. Since the relays measure the derivatives in the direction towards the middle of the cable, the reverse faults cause negative derivatives. Thus, the relays can distinguish the reverse faults from the forward faults and refrain from issuing trip signals for the reverse faults.

The purpose of this current derivative protection method is to detect and isolate the faulted cable using the PDs located at two ends. Therefore, a pick-up value must be defined so that only two relays on the faulted cable (with LRF) will measure current derivatives larger than the pick-up value, and the relays on the rest of the cables measure small values.There are two challenges in this method: (i) the current derivative for a fault right next to the relay (at 0% of cable length) is extremely large, which is theoretically infinity due to zero inductance in the RLC circuit, and therefore the relay cannot trip the faulted cable before the fault current gets too high; (ii) the current derivative for a fault at the remote end of the cable (at 100% of cable length) will be the smallest, and the pick-up value must be smaller than this derivative but should also be larger than the current derivative for a fault on the next cable segment.

To solve these challenges, current limiting inductors (CLIs) are used as shown in

Figure 4-1. A CLI is mounted between the PD and the end of the cable. With the current limiting inductance, Relay-A will not measure an ultra-large current derivative for fault F1 anymore, and the current derivative during fault F3 will be smaller than the current derivative during fault F2. With this arrangement, if a pick-up value is defined to satisfy the above two conditions, Relay-A in Figure 4-1 will only detect the faults on the cable it protects (between F1 and F2).

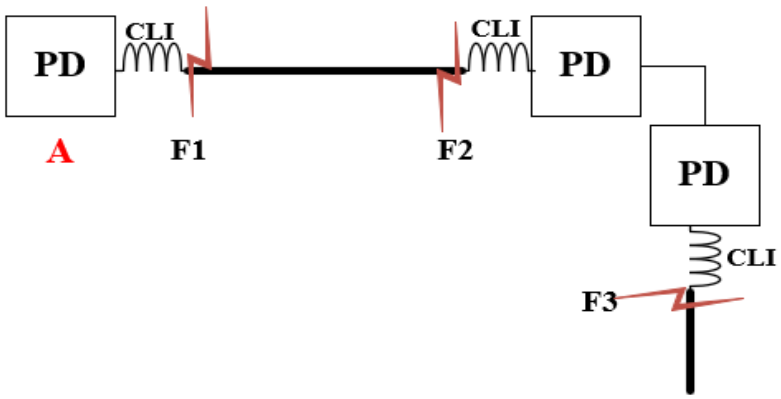

Figure 4-1: Current limiting inductors.

From (4-1) and (4-2), the current derivatives for a fault at the remote end of the protected cable can be calculated for the pick-up value selection. Table 4-1 shows the design parameters required for a sample calculation.

Table 4-1: Protection design parameters

Sampling Time Interval	CLI	V(0)	$R_{cable\text{-}100\%}$	$L_{cable\text{-}100\%}$
10 μs	10 μH	200 V	7 mΩ	30 μH

Using 10 μs calculation time step, the current derivative waveform for a 100 m cable is plotted in Figure 4-2. In (3-3), if α^2 is equal to ω_0^2, the system is in critical-damped. The corresponding critical resistance R_{crit} is calculated as 0.09 Ω. Since 0.09 Ω is considered as a low fault resistance, HRFs will always result in an over-damped response. In Figure 4-2, the variations of current derivatives for three different faults: (i) a 0.01 Ω LRF which results in an under-damped response, (ii) a 0.1 Ω LRF that results in an over-damped response, and (iii) a 5 Ω HRF that result in an over-damped response, are plotted. It can be seen from the graphs that the two LRF current derivative waveforms decay much slower compared to those of the HRF. Therefore, the current derivative protection method proposed in this chapter is only used for LRFs. To cover all possible LRFs during one sampling time interval, the current derivative at the first time step after the fault happens is selected as the pick-up value for relays. From both cases, the derivative values at the first time step are very close to and greater than 4.88 MA/s. Thus, 4.88 MA/s is set as the pick-up value.

In Figure 4-3, the LRF detection algorithm of each relay is illustrated. When an LRF happens on a cable, only the relays protecting the faulted cable will measure two current derivatives which are larger than the pick-up value. As a result, the fault will be cleared by these relays. To examine its protection speed and selectivity, simulations are performed in the next section.

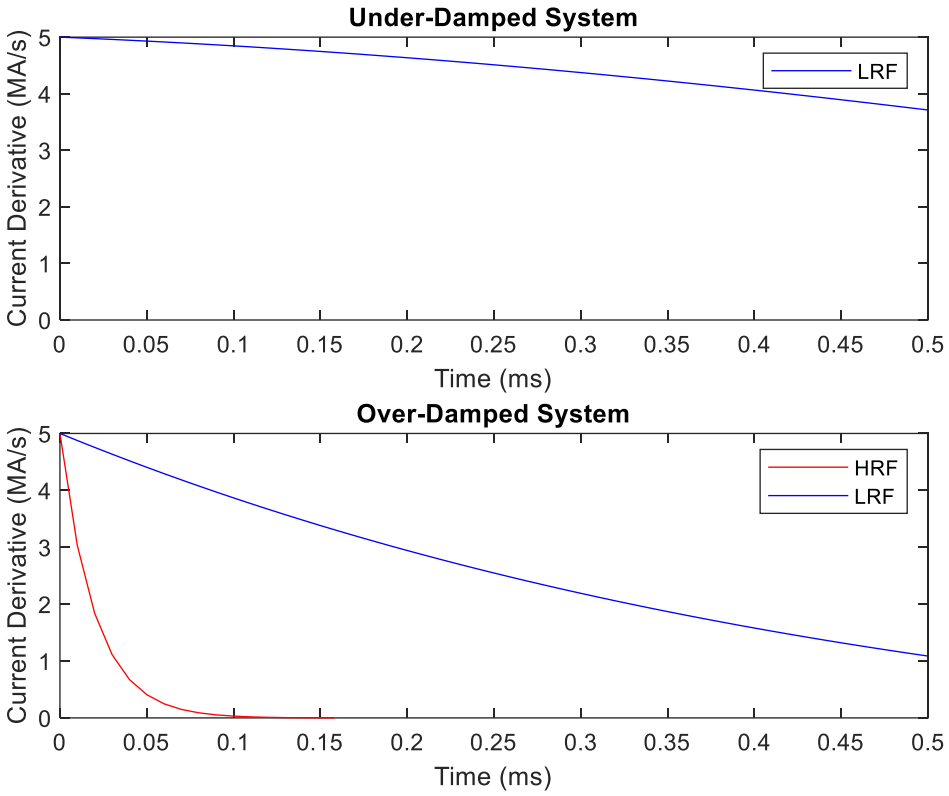

Figure 4-2: Fault current derivative waveforms.

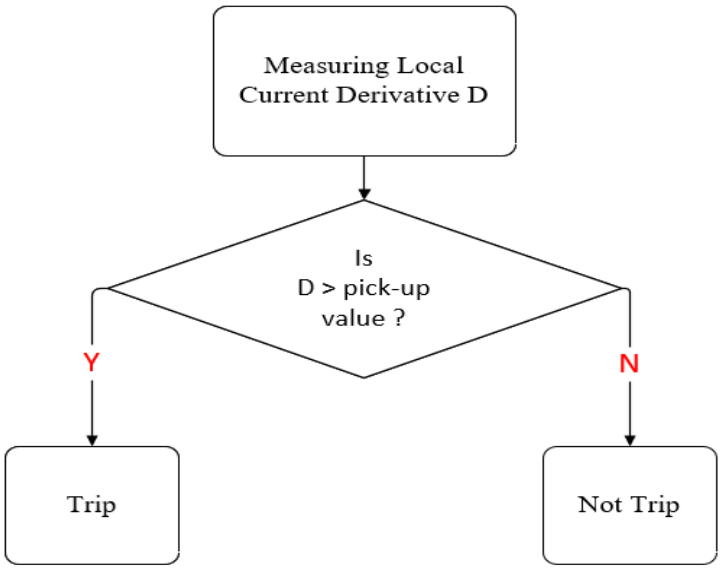

Figure 4-3: Protection algorithm of LRFs.

4.3 Simulation Results

In this section, the proposed LRF detection method is applied to the DCMG described in Figure 3-10. Three different types of simulations were performed using the PSCAD simulation model of the DCMG to test the reliability of the proposed current derivative protection method.

4.3.1 Change of Modes

In the current derivative protection, relays must only respond to faults. Any transient waveforms caused by normal operational actions such as change of operating mode should not be detected as faults. In this simulation, the model was switched from the grid-connected mode to the islanded mode at time 1.11 s and switched back at time 1.6 s.

As shown in Figure 4-4, during two change of mode periods, current derivatives measured by all relays do not exceed the pick-up value 4.88 MA/s. Therefore, change of mode operations will not be detected as faults.

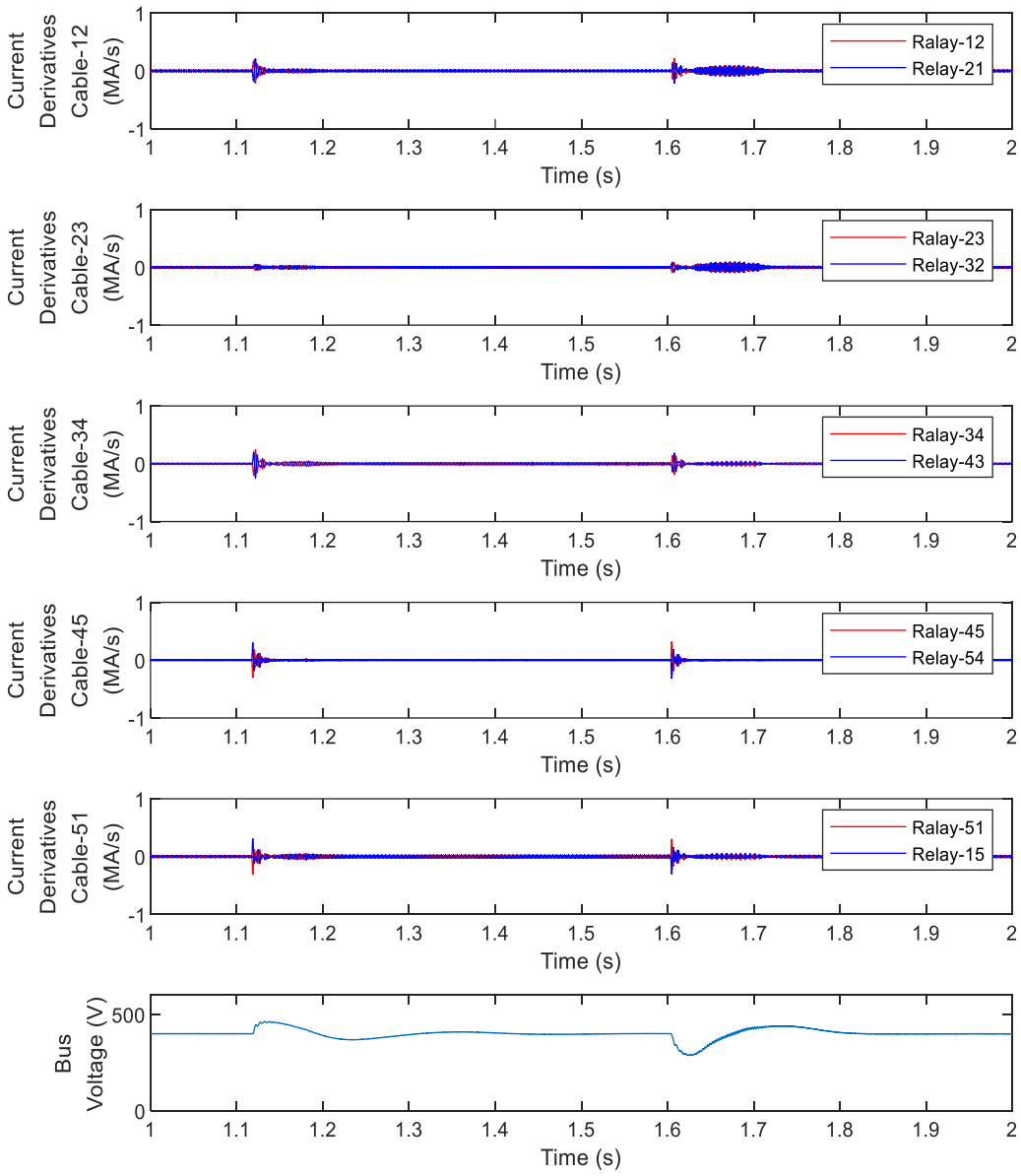

Figure 4-4: Variations of the current derivatives at relay points during change of modes.

4.3.2 Faults in the Grid-connected Mode

In this section, the simulations were performed when the DCMG was in the grid-

connected mode.

In this simulation, a PG LRF with 0.01 Ω resistance was applied on Cable-12, at 10% of the cable length (10 m) from Bus-1 side at time 1.0 s. According to the protection algorithm, two relays on Cable-12 should detect high current derivatives immediately after the fault inception. Other relays should measure very small derivatives, mainly due to the effect of CLIs.

As shown in Figure 4-5, only Relay-12 (Bus-1 side) and Relay-21 (Bus-2 side) measure current derivatives which are greater than the pick-up value. Table 4-2 collects the trip status from all relays. As the faulted cable is correctly tripped by Relay-12 and Relay-21, the DC bus voltage is maintained at 400 V. This can be seen in Figure 4-6. The protection speed is fast enough that the fault current only reaches 300 A.

Table 4-2: Trip signals for the PG fault on Cable-12 at 10% from Bus-1

Relay	12	21	23	32	34	43	45	54	51	15
Trip	1	1	0	0	0	0	0	0	0	0
1 - tripped; 0 - did not trip										

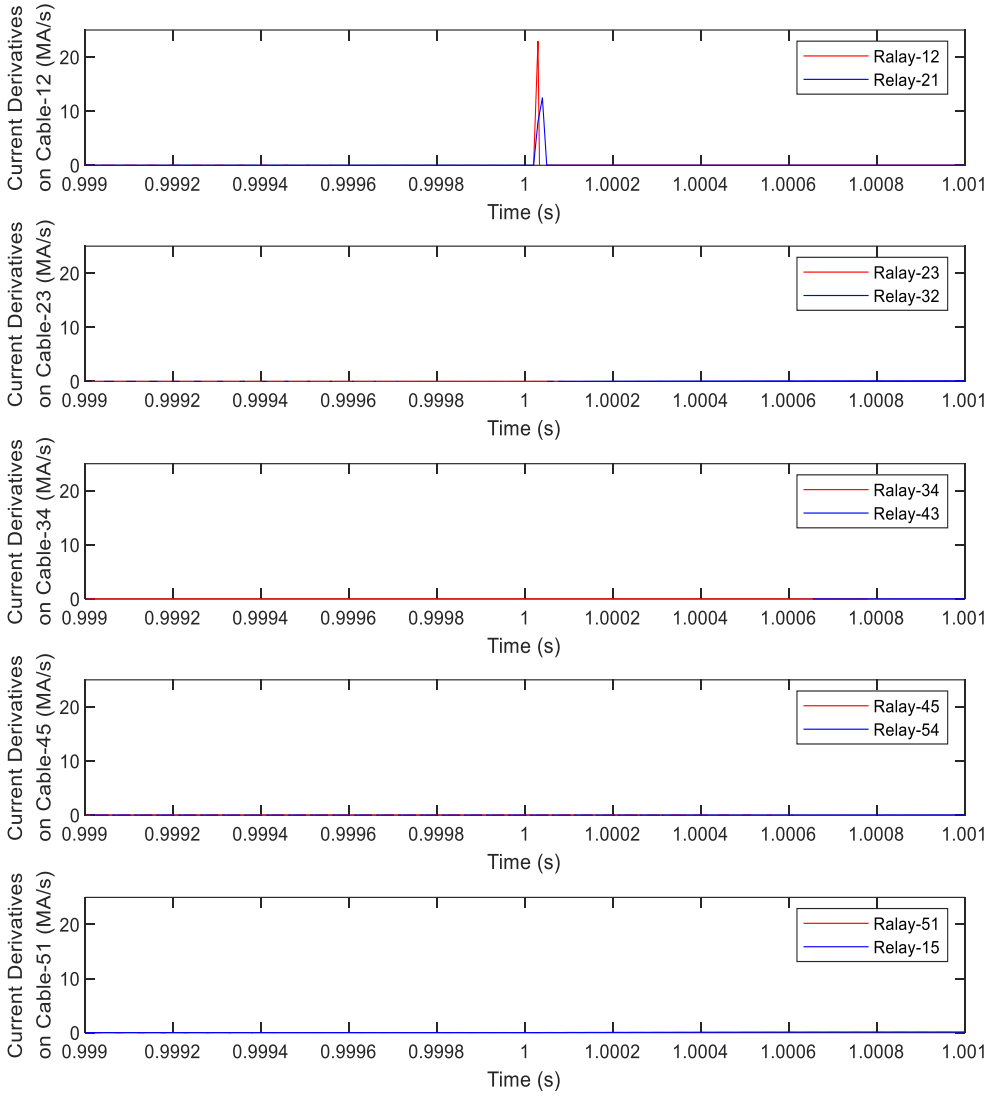

Figure 4-5: The current derivatives at different relays for a PG LRF on Cable-12 at 10% distance from Bus-1.

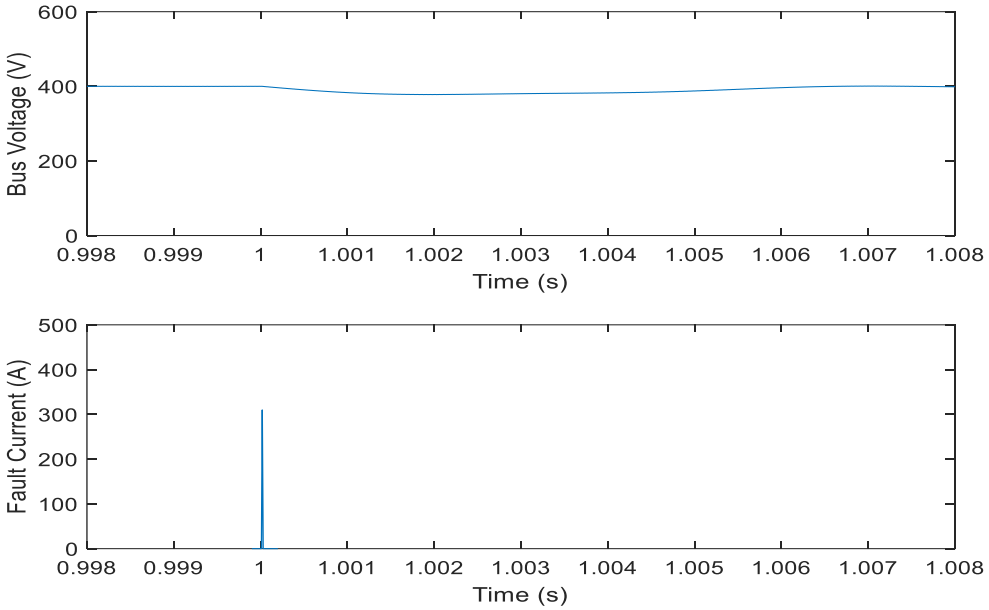

Figure 4-6: The bus voltage and the fault current corresponding to the PG fault shown in Figure 4-5.

4.3.3 Faults in the Islanded Mode

In this section, the simulations were performed with the DCMG operating in the islanded mode.

In this simulation case, a PP LRF with 0.09 Ω resistance was applied at 1.0 s on Cable-51, next to Relay-51 (0% from Bus-5). Theoretically, Relay-51 (Bus-5 side) and Relay-15 (Bus-1 side) should trip the cable.

As illustrated in Figure 4-7, Relay-15 and Relay-51 have correctly detected current derivatives higher than the pick-up value during the fault, while other relays do not observe current derivatives which are higher than the pick-up. Table 4-3 lists trip signals

from all relays under the low resistance PP fault. As Relay-15 and Relay-51 cleared the faulted cable almost instantaneously. As a result, the bus voltage was well maintained around 400 V, and the fault current peak was limited to only 350 A, as shown in Figure 4-8.

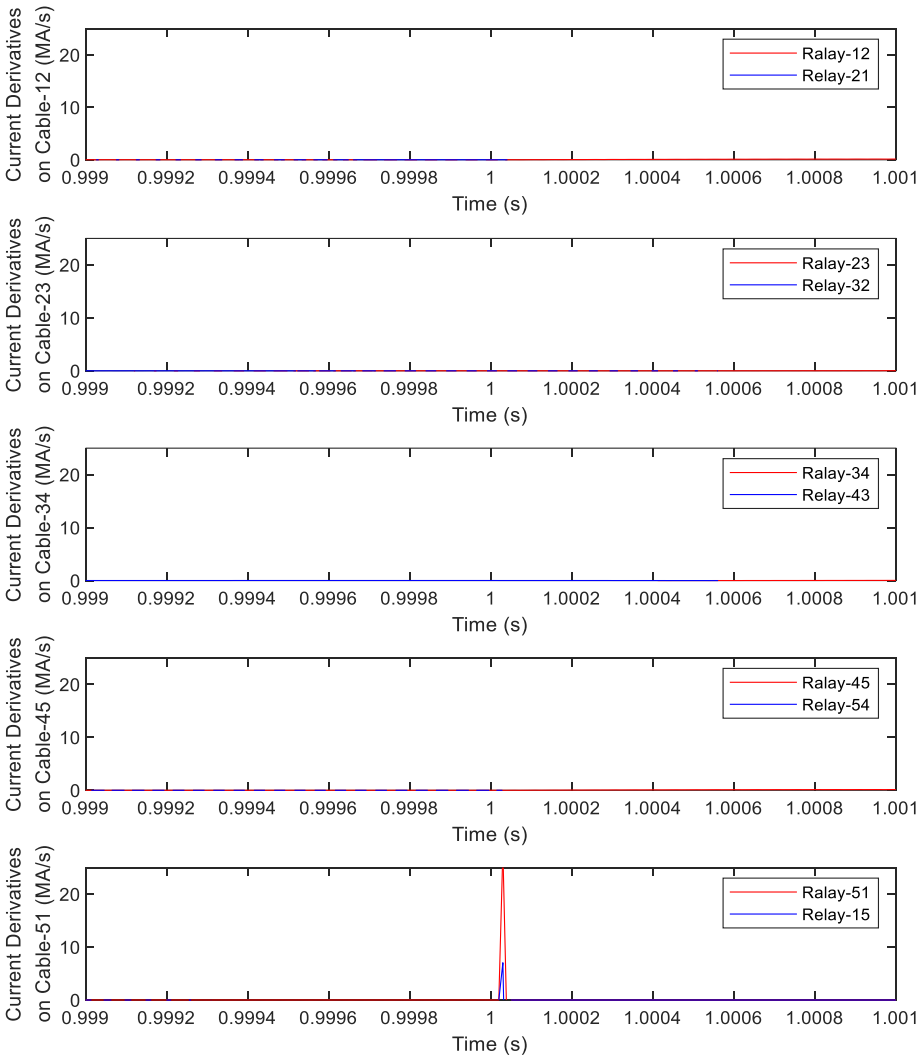

Figure 4-7: The current derivatives at different relays for a PP fault on Cable-51 next to Bus-5.

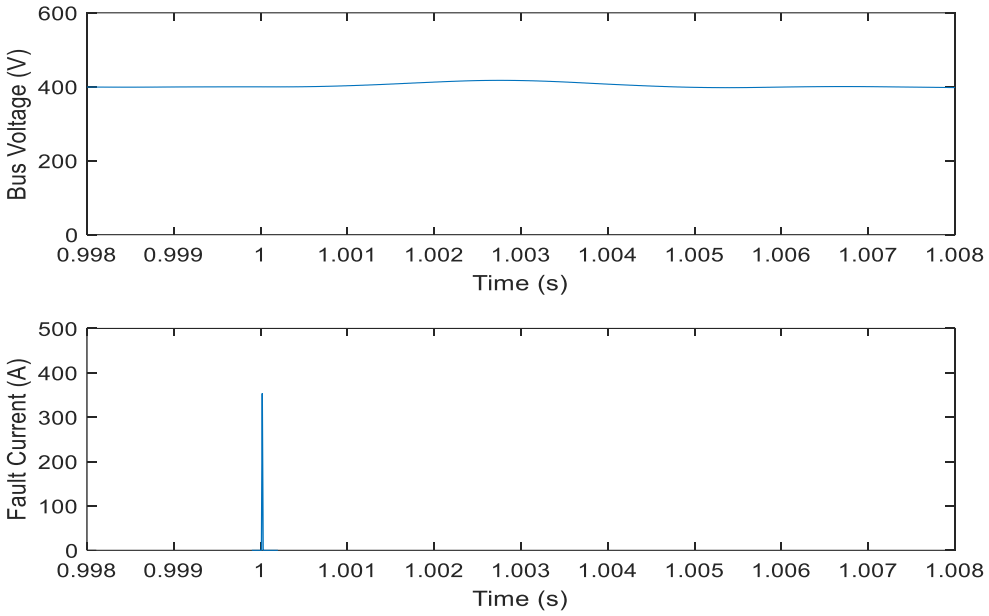

Figure 4-8: The bus voltage and the fault current corresponding to the PP fault shown in Figure 4-7.

Table 4-3: Trip signals for the PP fault on Cable-51 at 0% distance from Bus-5

Relay	12	21	23	32	34	43	45	54	51	15
Trip	0	0	0	0	0	0	0	0	1	1
1 - tripped; 0 - did not trip										

4.4 Summary

Chapter 4 proposed a DCMG protection scheme to detect and clear LRFs. The scheme uses current derivative protection with local measurements. From the time domain equation derived in Chapter 3, current derivative equations were obtained in this

chapter. By exploring the attenuation trend of the fault current derivative, an appropriate pick-up value was selected. When the relay reads a derivative higher than the pick-up value, it trips the cable. Moreover, CLIs are mounted to guarantee enough operating time for the near-point fault and to avoid operation to the fault on the other cable.

Simulations were done to examine the reliability of this protection scheme for LRFs. From the results, the system can successfully clear both PP and PG faults when the model is in both modes without mal-functions during the change of mode periods. At the same time, the model keeps working normally. The protection speed and selectivity are proven. To complete the DCMG protection scheme, HRFs must also be well handled. In the next chapter, a unit protection method is designed to detect HRFs.

Chapter 5 Detection and Discrimination of High Resistance Faults

5.1 Introduction

Compared to LRFs, high resistance faults (HRFs) have small current derivatives due to high fault resistances. Although an HRF may have a safe steady-state fault current, and the system under the fault can even operate normally, the HRF must be eliminated, because in some cases the initial RLC responses can still cause large initial fault currents, and the unfaulty cables will be subjected to overvoltage stresses under PG faults.

High fault resistances result in higher α values in the expressions for fault current derivatives given in (4-1) and (4-2). This will result in fast attenuation of fault current derivatives. As shown in Figure 4-2, the red curve representing current derivatives of HRFs decay fast. Therefore, the protection method proposed in Chapter 4 cannot detect HRFs. If a smaller pick-up value is chosen, mal-operations will happen; an LRF on the remote bus or the next cable segment in the forward direction can be confused with an HRF near the relay as the resulting current derivatives are similar. Therefore, the current derivative method with local measurements is not suitable for detecting and discriminating HRFs.

Fortunately, due to high fault resistances, HRFs have small current derivatives. Compared to LRFs that need fast protection speed, fault currents of HRFs rise slowly.

Therefore, the protection speed is not the major challenge. Since unit protection methods can satisfy the protection selectivity easily, and their communication delays are not a major concern in the case of HRFs, in this chapter, a unit protection is proposed to detect and discriminate HRFs.

5.2 Unit Protection Method

According to Kirchhoff's Current Law (KCL), currents flowing in and out of a cable must be the same. Therefore, on a healthy cable, the currents measured by relays at both sides must have the same magnitude and different signs, because the directions of measurement at both ends is usually towards the cable from the bus. Then, their derivatives must follow the same characteristics.

A unit protection method can be designed based on current derivatives. Since on a healthy cable, the relays at its two ends must measure opposite current derivatives, the no fault condition on the cable is expressed as:

$$\frac{\mathrm{D1}}{\mathrm{D2}} = -1 \tag{5-1}$$

where D1 and D2 are current derivatives at both ends of the cable.

When a fault is applied on the cable, fault currents generated by discharging filtering capacitors at both sides flow into the cable, causing two positive current derivatives at both sides. As a result, the ratio of two derivatives is a positive value. Thus, during a fault condition:

$$\frac{D1}{D2} > 0. \quad (5\text{-}2)$$

With (5-2), using a communication link to gather the current derivatives of both relays, an algorithm can be developed for detection of the HRFs as illustrated in Figure 5-1. During a fault, only the two relays on the faulted cable can calculate positive derivative ratios. Rest of the relays must all have minus one ratio.

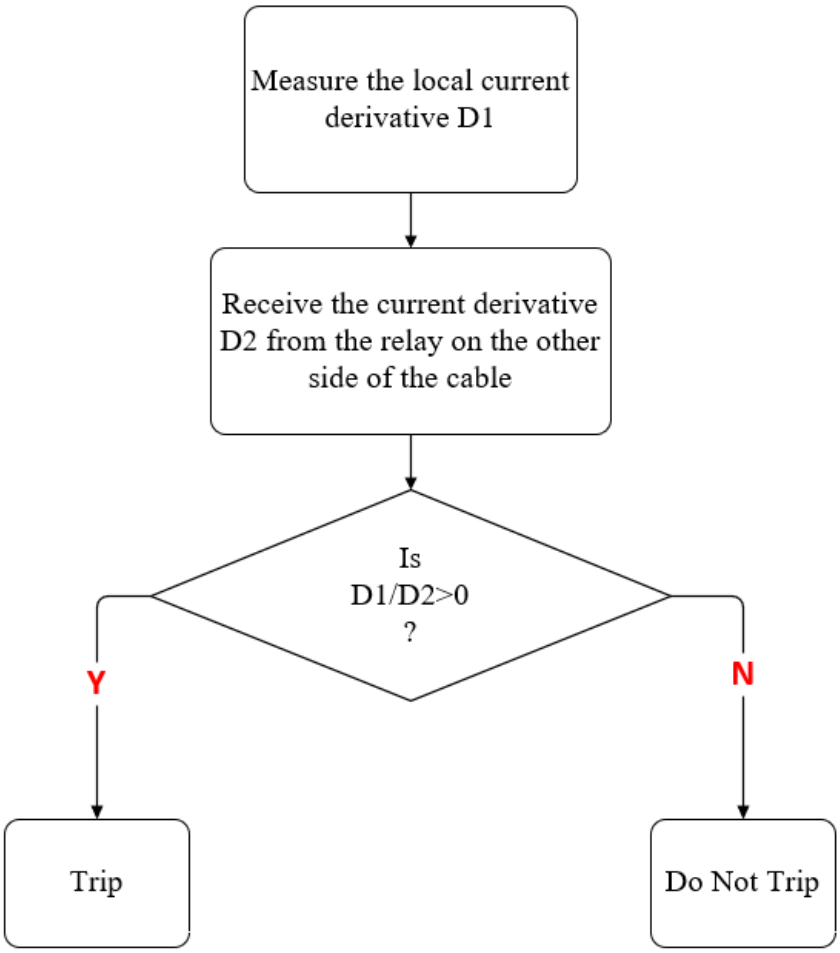

Figure 5-1: Protection algorithm of HRFs.

5.3 Simulation Results

To prove the reliability of the unit protection, different faults were applied under

different operating modes of a ring bus DCMG using PSCAD.

5.3.1 Faults in the Grid-connected Mode

In this case, the DCMG model was in the grid-connected mode. A PP HRF with 1 Ω resistance was applied on Cable-45 at 1.0 s, at 40% of the cable length (40 m) from Bus-5.

As shown in Figure 5-2, after 20 μs communication delay, the current derivative ratios calculated in Relay-45 (Bus-4 side) and Relay-54 (Bus-5 side) change from minus one to positive values, while other relays still have a negative ratio.

In Table 5-1, the corresponding trip signals are presented. Only Relay-45 and Relay-54 issued trip signals. The protection selectivity is correct.

In Figure 5-3, which shows the variation of DC bus voltage, it can be seen that the DC bus voltage is regulated at 400 V. The fault current reached only to 180 A before the fault is cleared. Therefore, the protection speed is also satisfied. The system remains stable.

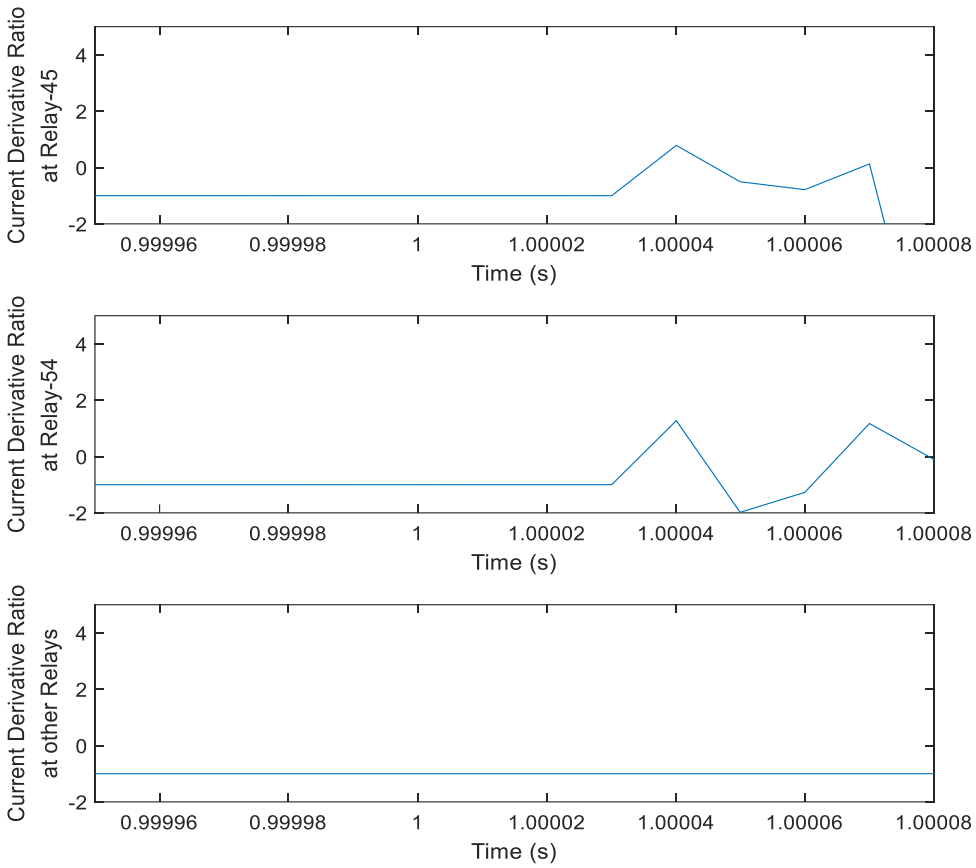

Figure 5-2: The current derivative ratios (D_1/D_2) at different relays for a PP fault on Cable-45 at 40% distance from Bus-5.

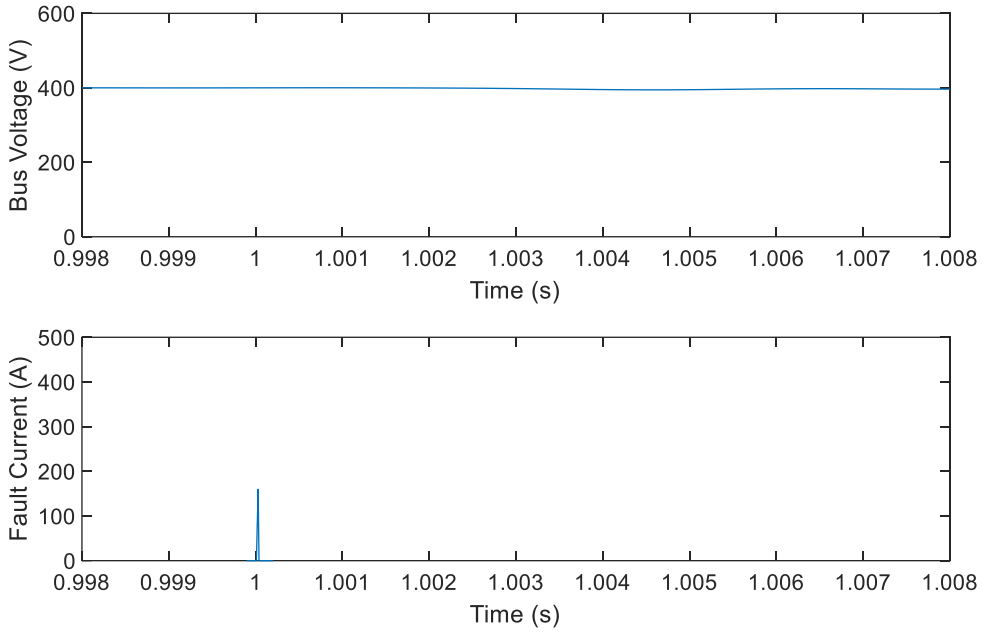

Figure 5-3: The bus voltage and the fault current corresponding to the PP fault shown in Figure 5-2.

Table 5-1: Trip signals for the PP HRF on Cable-45 at 40% distance from Bus-5

Relay	12	21	23	32	34	43	45	54	51	15
Trip	0	0	0	0	0	0	1	1	0	0
1 - tripped; 0 - did not trip										

5.3.2 Faults in the Islanded Mode

In this section, the protection scheme was tested under the islanded mode.

At time 1.0 s, a PG HRF with 5 Ω resistance is applied on Cable-23, next to Relay-23 (0% from Bus-2). According to the protection algorithm, only Relay-23 (Bus-2 side)

and Relay-32 (Bus-3 side) could detect this internal fault.

As shown in Figure 5-4, Relay-23 and Relay-32 have detected the fault as expected since they have positive current derivative ratios. The rest of the relays have a negative ratio.

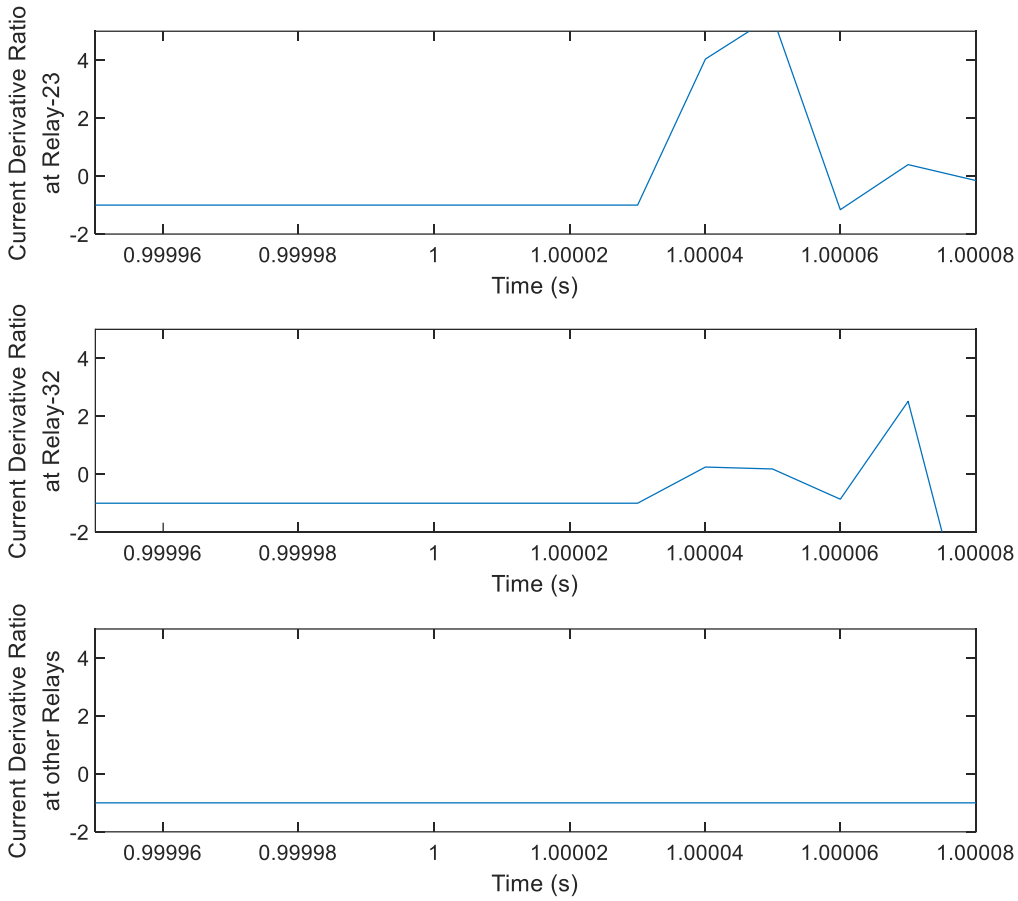

Figure 5-4: The current derivative ratios (D_1/D_2) at different relays for a PG fault on Cable-23 next to Bus-2.

In Figure 5-5, the bus voltage is maintained at 400 V, and the fault current is below 50 A. This simulation proves the protection speed and selectivity.

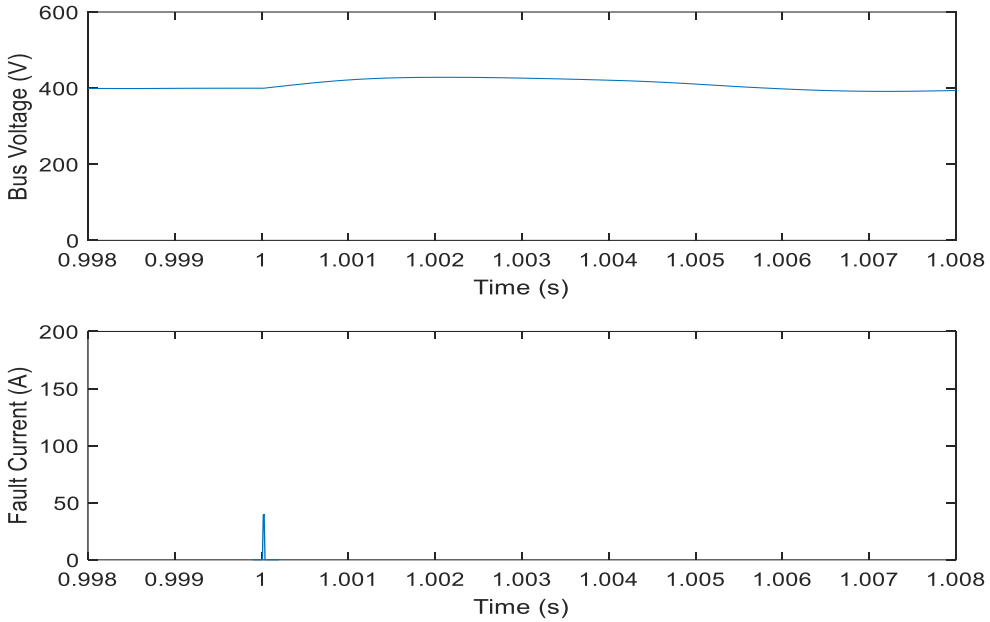

Figure 5-5: The bus voltage and the fault current corresponding to the PG fault shown in Figure 5-4.

As confirmed in Table 5-2, only Relay-23 and Relay-32 trip the cable.

Table 5-2: Trip signals for the PG HRF on Cable-23 at 0% from Bus-2

Relay	12	21	23	32	34	43	45	54	51	15
Trip	0	0	1	1	0	0	0	0	0	0
1 - tripped; 0 - did not trip										

5.4 Special Tests on Integrated Protection Scheme

In this section, LRF and HRF protection methods are integrated and tested under two special situations to further investigate the reliability of the proposed protection scheme.

5.4.1 N-1 Contingency Tests

In the first situation, one cable was initially isolated from the ring bus DCMG in Figure 2-2 to form an N-1 contingency, and the protection scheme was tested for various faults. The N-1 contingency will change the ring bus DCMG into a radial system. The integrated protection scheme was tested whether it can work for the radial systems as well.

In the first case, Cable-45 was tripped initially. A PG LRF with 0.1 Ω resistance was applied on Cable-51 next to Bus-1. As shown in Figure 5-6, the fault was detected by Relay-15 and Relay-51. The faulted Cable-51 was successfully tripped. At this time, Cable-45 and Cable-51 were both isolated from the system. Thus, the battery was disconnected. From the graph, the bus voltage was maintained at 400 V. The system did not crash.

In the second case, Cable-51 was tripped initially. A PP HRF with 2 Ω resistance was applied on Cable-12 next to Bus-2. As shown in Figure 5-7, only Relay-12 and Relay-21 detected the fault, while other relays only measured negative ratios. Thus, the fault on Cable-12 was cleared. At this time, Cable-12 and Cable-51 were isolated from the system, and the PV source was disconnected from the ring bus DCMG. From the graph, the bus voltage was maintained at 400 V. The system was working normally.

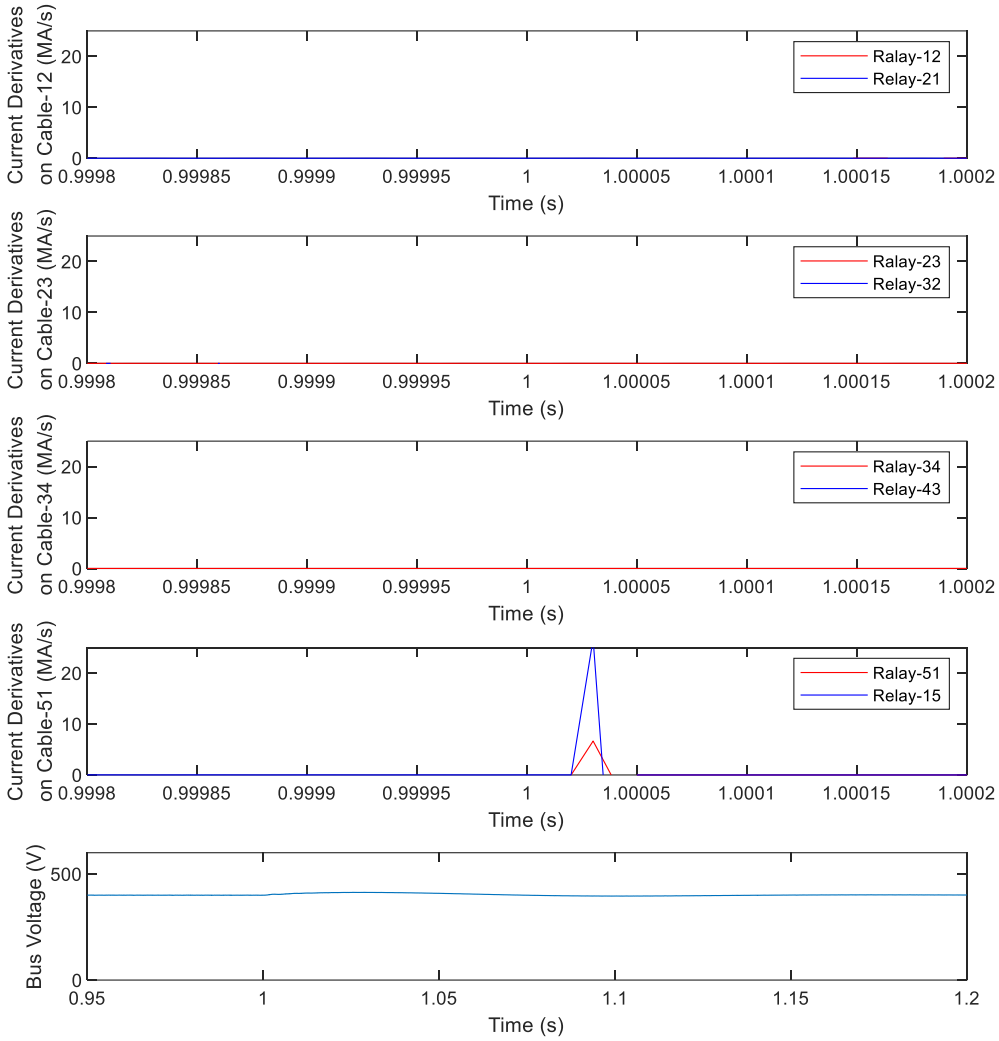

Figure 5-6: The current derivatives at different relays and the bus voltage for a PG fault on Cable-51 next to Bus-1 when Cable-45 was initially tripped.

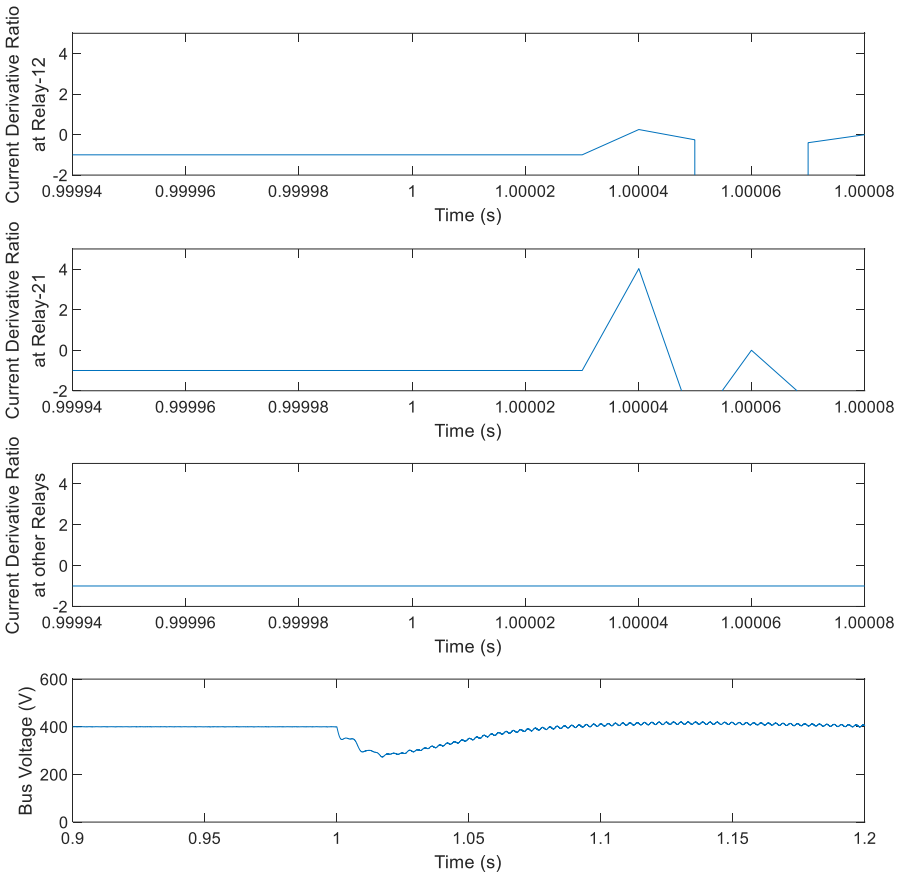

Figure 5-7: The current derivative ratios (D_1/D_2) and the bus voltage for a PP fault on Cable-12 next to Bus-2 when Cable-51 was initially tripped.

5.4.2 Noise Tests

In the second situation, noise signals were injected to relays. Now, the measured currents will contain significant errors. The protection scheme was tested to various noise signals and explored how much noise the protection system can sustain.

A simple noise generator is designed and shown in Figure 5-8. The measured cable currents with noise are the sum of the original cable current and the noisy current. A

random number generator with the limit from -1 to 1 provides a noise factor (NF) using Gaussian distribution with standard deviation of 2 at each time step. The noisy current is calculated as:

$$I_{noisy} = I_{cable} / SNR * NF. \quad (5\text{-}3)$$

Therefore, the measured current by relay is expressed as:

$$I_{relay} = I_{cable} + I_{noisy}. \quad (5\text{-}4)$$

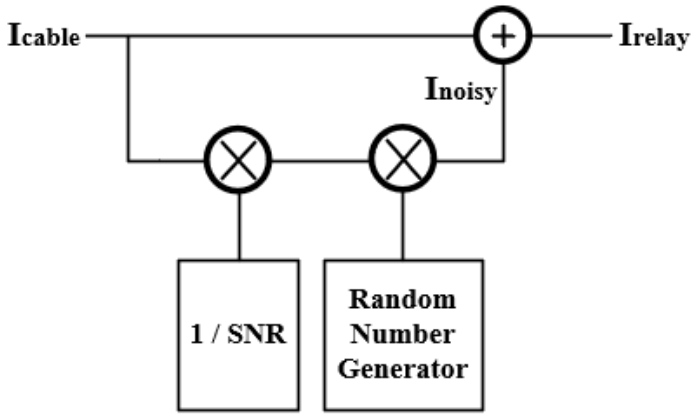

Figure 5-8: Noise generator.

A PG LRF with resistance 0.01 Ω was applied on Cable-12 next to Bus-1. The system was tested by various noise signals with different SNRs. As shown in Table 5-3, when SNR(dB) is smaller than 40 dB, the noisy current under steady-state becomes large enough so that it can cause mal-operations of the relays.

Table 5-3: The operation status of the relays under various noises

SNR(dB)	50	45	40	35

Relay	Normal	Normal	Normal	Mal-operation

The result of the noise with 40 dB SNR is shown in Figure 5-9. The current derivatives measured by the relays contains obvious oscillating components. During the steady-state, the current derivatives did not exceed the pick-up value. When the fault happened, Relay-12 and Relay-21 successfully detected the fault under noise environment.

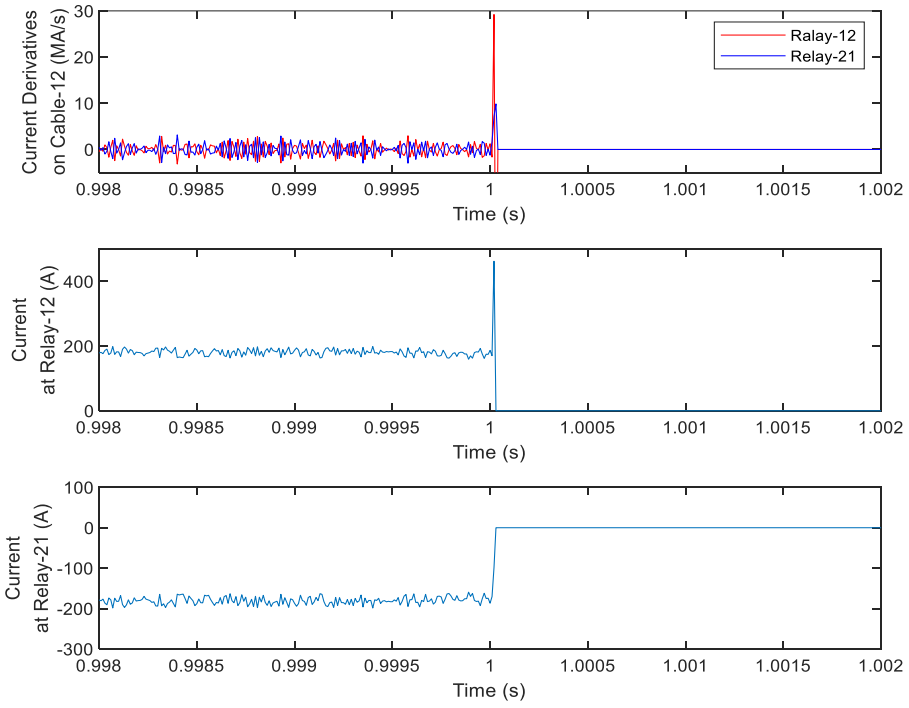

Figure 5-9: The current derivatives and the currents measured by the relays on the faulted cable under noise situation.

5.5 Summary

In this chapter, a protection method for detecting HRFs is discussed. A convenient unit protection method based on the Kirchhoff's Current Law but using the current derivatives is proposed. By calculating the ratio of current derivatives at two ends of the cable, relays can detect HRFs without confusing with LRFs.

This method can also detect LRFs. Due to communication delay, the local measurement method in the previous chapter works faster than this unit protection method. Therefore, the unit protection method can also work as a backup protection for LRFs. With both methods operate together in parallel, the ring bus DCMG can detect and discriminate both LRFs and HRFs with critical design requirements, the speed and selectivity requirements satisfied. The complete protection scheme can give a robust response under significance measurement noise and different pre-fault network configurations without having to adjust any settings.

Chapter 6 Cable Fault Location

6.1 Introduction

In Chapters 4 and 5, a complete DCMG fault protection scheme was developed. When there is a permanent fault on a cable, it must be located and repaired before the faulted cable is brought back into service. If the accurate fault location on the faulted cable can be found using the measurements made during the fault, the repairs can be carried out faster and efficiently. In this chapter, a mathematical approach is proposed to quickly calculate the fault location.

6.2 Fault Location Calculation Method

Considering the initial values of the current derivatives given by (4-1) and (4-2), the initial rate of change of current can be obtained as:

$$\frac{di}{dt}\Big|_{t=0} \approx \frac{V(0)}{L}. \tag{6-1}$$

The expression given in (6-1) is applicable for both under-damped and over-damped cases. The accuracy of this equation depends on the equivalent resistance in the RLC response. For HRFs, this equation can have errors. However, the ratio of two derivatives on the same faulted line can effectively reduce the error.

According to the unit protection method using current derivative ratios from Chapter 5, relays will only trip the signal when they calculate positive derivative ratios. The first

positive current derivative ratio can be used to make an approximation to the fault location. Substituting (6-1) into (5-2), current derivative ratios calculated by relays can be expressed as:

$$\frac{D1}{D2} \approx \frac{L2}{L1} \tag{6-2}$$

Where L1 and L2 are the equivalent inductances at both sides of the fault location. In this model, the equivalent inductance at each side is the sum of part of the cable inductance and a current limiting inductance. Therefore, the sum of the L1 and L2 is the total cable inductance plus two limiting inductances:

$$L1 + L2 = L_{cable} + 2L_{CLI}. \tag{6-3}$$

Solving (6-2) and (6-3) results in expressions of L1 and L2:

$$L1 = \frac{Lcable+2L_{CLI}}{\frac{D1}{D2}+1} \tag{6-4}$$

$$L2 = \frac{Lcable+2L_{CLI}}{\frac{D2}{D1}+1}. \tag{6-5}$$

Fault location equations defined by the cable percentage length are:

$$\text{Fault Location (Relay 1)} = \frac{L1-L_{CLI}}{Lcable} \tag{6-6}$$

$$\text{Fault Location (Relay 2)} = \frac{L2-L_{CLI}}{Lcable}. \tag{6-7}$$

From (6-6) and (6-7), two estimates can be obtained for the fault location with respect to the relays at two ends of the faulted cable. By comparing the two location values, the accuracy of the location can be further improved.

6.3 Simulation Results

To test the accuracy of the fault location calculation method, simulations were performed for both LRF and HRF cases.

6.3.1 Low Resistance Fault Test

The fault location method was first applied to an LRF simulation case. At time 1.0 s, a PG LRF with 0.1 Ω resistance was applied on Cable-51 next to Relay-51 (0% from Bus-5).

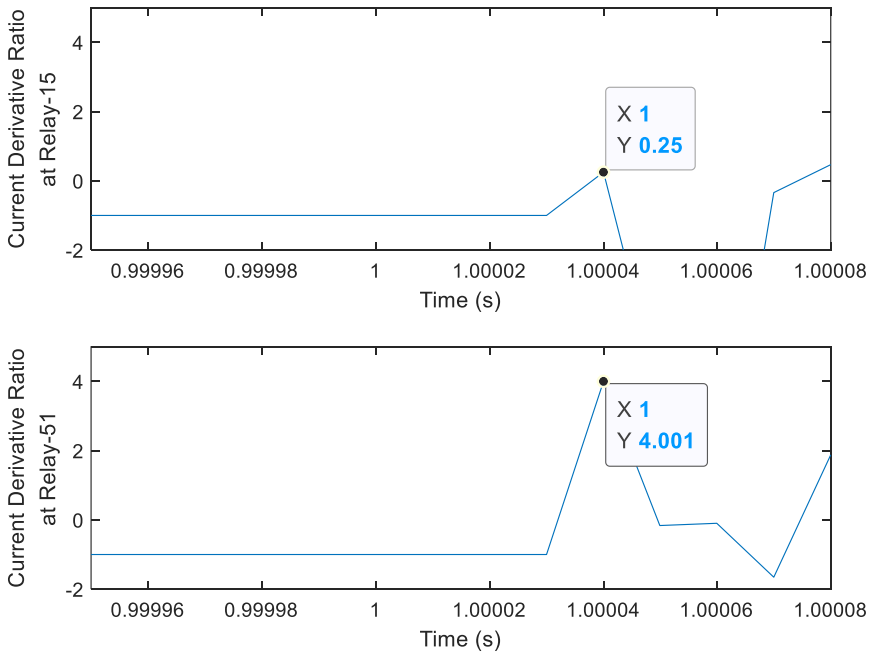

Figure 6-1: The current derivative ratios for PG LRF on Cable-51 at 0% distance from Bus-5.

As shown in Figure 6-1, the first positive ratio in Relay-15 (Bus-1 side) is 0.25; the

first positive ratio in Relay-51 (Bus-5 side) is 4.001. Using (6-4) and (6-5), equivalent inductances at Relay-15 side (L1) and Relay-51 side (L2) are 40 μH and 10 μH respectively. Substituting two inductances into (6-6) and (6-7), the fault location calculated by Relay-15 is 100% (0% referred to Relay-51 side), and the location calculated by Relay-51 is 0%. The results are consistent with the actual location.

6.3.2 High Resistance Fault Tests

Two HRF tests were done in this section.

In the first case, a PG HRF with 2 Ω resistance was applied on Cable-12 at 20% (20 m) away from Bus-2 at time 1.0 s. The DCMG worked in the grid-connected mode.

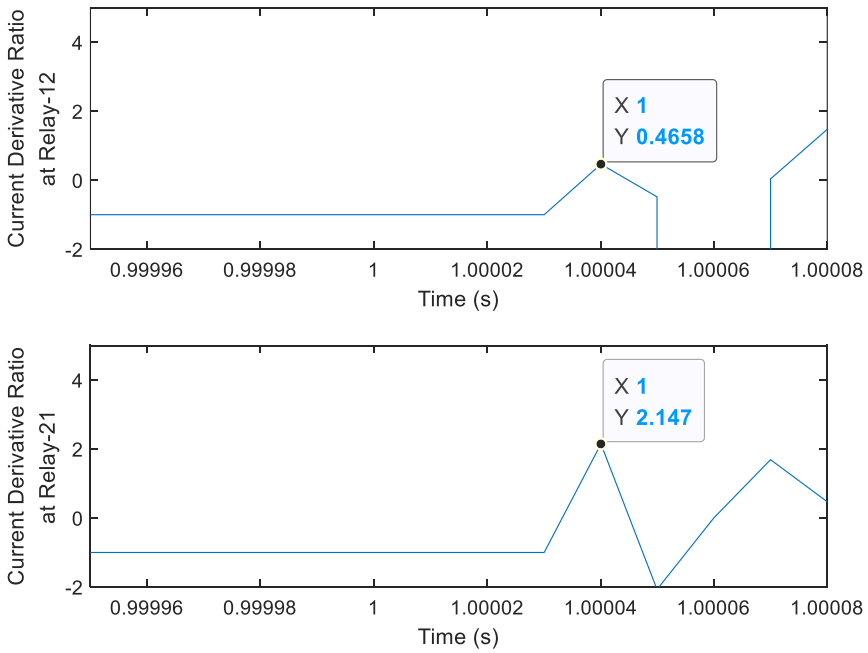

Figure 6-2: The current derivative ratios for the PG HRF on Cable-12 at 20% distance from Bus-2.

From Figure 6-2, first positive current derivative ratios of Relay-12 (Bus-1 side) and Relay-21 (Bus-2 side) are 0.4658 and 2.147 respectively. Using (6-4) and (6-5), the equivalent inductances at two sides are obtained as L1 = 34.1 μH and L2 = 15.9 μH. The fault locations calculated using (6-6) and (6-7) are 80.33% (relay-12 side, which is 19.67% referred to Bus-2 side) and 19.67% (Relay-21 side). Compared to the actual location 20% (Bus-2 side), the error is negligible.

In the second test, a PP HRF with 2 Ω resistance was applied at the middle of Cable-51 (50% from either side) at time 1.0 s. The DCMG was in the islanded mode.

In Figure 6-3, 0.9993 and 1.001 are first positive current derivative ratios detected by Relay-51 and Relay-15 respectively. By (6-4) and (6-5), the equivalent inductances are L1 = 25.01 μH (Relay-51 side) and L2 = 24.99 μH (Relay-15 side). Using (6-6) and (6-7), the fault locations calculated by Relay-51 and Relay-15 are 50.03% and 49.97% respectively. These are consistent with the actual location 50%.

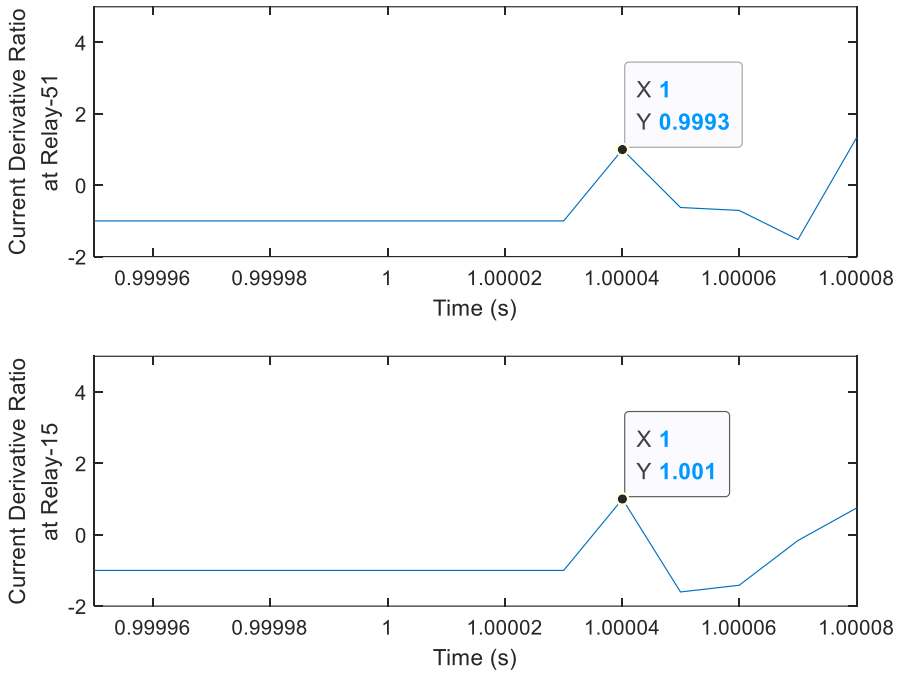

Figure 6-3: The current derivative ratios for PP HRF at the middle of Cable-51.

6.4 Summary

In this chapter, a method to determine the fault location on a cable was proposed. The algorithm is derived from the unit protection method proposed in Chapter 5. The cable inductance between the relay and the fault is calculated from the current derivative ratio. Three simulation cases involving both LRFs and HRFs were presented , and their results have proven the accuracy of the calculation.

A complete protection scheme for a ring bus DCMG has been developed with the algorithms presented in Chapters 4, 5 and 6. It can detect and clear LRFs and HRFs in either of the DCMG operation modes, and effective for both PG and PP faults. In addition, the approximate locations of the faults can be determined.

Chapter 7 Conclusions and Future Work

7.1 Conclusions

This thesis proposed and simulated a new protection scheme for a ring bus DCMG. The characteristics of DCMGs, including their configurations, control systems and operating modes were reviewed. Based on the literature review, a model of a ring bus DCMG was developed and implemented on PSCAD. Using the developed DCMG model, characteristics of DCMG faults were studied. Some protection devices such as grounding circuits, current limiting inductors and SSCBs were also introduced to the DCMG simulation model. In addition, simplified mathematical expressions that described the initial variations of the fault currents and their derivatives were derived by applying the Laplace transformation to series RLC circuits that approximately represent a DCMG during the initial phase of a fault. The analytical calculations with the parameters of the DCMG considered in the thesis showed that HRFs always result in an over-damped fault current response, while LRFs result in an under-damped response. In the case of over-damped response, the derivative of the current falls rapidly, while that remains high for a comparatively longer period when the response is under-damped. These characteristics were confirmed by the simulation results. Moreover, in both cases the initial rate of change of current is determined by the initial DC voltage and the equivalent inductance of the faulted circuit.

The rest of the thesis was devoted to developing the protection algorithms. Unlike most previous researches that use complicated systems to detect both LRFs and HRFs, this thesis combines two different protection methods to protect the DCMG under LRFs and HRFs. A current derivative protection with local measurements was proposed for detecting LRFs. A unit protection with current derivative ratios was designed for detecting HRFs. The combination of these two methods has satisfied the design challenges of protection speed for LRFs and protection selectivity for HRFs. Additionally, a fault location method that uses current derivative ratios was also introduced. With all three parts together, a strong protection system was established.

To prove the stability and reliability of the proposed protection scheme, many simulations were performed. The scheme operated well without any mal-operations and fulfilled all protection objectives. Furthermore, the protection scheme has a robust response under significance measurement noise and pre-fault network configurations corresponding to N-1 contingencies.

7.2 Future Work

In this research, the designed fault detection and localization system is mainly used to protect a ring bus DCMG under normal operations. Future work can be done to improve the protection coverage and reliability of the system:

- In this research, current derivatives were computed using sampled values of currents,

and a 100 kHz sampling rate was used. It is possible to explore direct measurement of current derivatives using Rogowski coils.

- Protection of faults under some critical situations can be analyzed. For example, faults happening during system transient states such as generation curtailment, battery SOC outside of the normal range and load shedding can be considered.
- Although the unit protection method can work as a backup protection system of the current derivative protection method when detecting LRFs, there is no backup protection system for the unit protection for HRFs. The secondary protection for HRFs is a new challenge.

Besides the above suggestion, other research work like control system improvements and design of SSCB snubber circuit with MOV can also be performed in the future.

References

[1] H. Bentarzi, R. A. Chentir, and A. Ouadi, “A new approach applied to steam turbine controller in thermal power plant,” in *the 2nd International Conference on Control, Instrumentation and Automation*, pp. 236-240, Dec. 2011.

[2] A. Qazi, F. Hussain, N. ABD. Rahim, G. Hardaker, D. Alghazzawi, K. Shaban, and K. Haruna, “Towards sustainable energy: A systematic review of renewable energy sources, technologies, and public opinions,” in *IEEE Access*, vol. 7, pp. 63837-63851, May 2019.

[3] K. Jia, Z. Yang, Y. Fang, T. Bi, and M. Sumner, “Influence of inverter-interfaced renewable energy generators on directional relay and an improved scheme,” in *IEEE Transactions on Power Electronics*, vol. 34, pp. 11843-11855, Dec. 2019.

[4] J. Feng, B. Zeng, D. Zhao, G. Wu, Z. Liu, and J. Zhang, “ Evaluating demand response impacts on capacity credit of renewable distributed generation in smart distribution systems,” in *IEEE Access*, vol. 6, pp. 14307-14317, Sept. 2017.

[5] D. Kumar, F. Zare, and A. Ghosh, ‘‘DC microgrid technology: System architectures, AC grid interfaces, grounding schemes, power quality, communication networks, applications, and standardizations aspects,’’ in *IEEE Access*, vol. 5, pp. 12230-12256, Jun. 2017.

[6] A. Hooshyar, E. F. El-Saadany, and M. Sanaye-Pasand, “Fault type classification in

microgrids including photovoltaic DGs," in *IEEE Transactions on Smart Grid*, vol. 7, pp. 2218-2229, Sept. 2016.

[7] C. Huang, F. Li, and Z. Jin, "Maximum power point tracking strategy for large-scale wind generator systems considering wind turbine dynamics," in *IEEE Transactions on Industrial Electronics*, vol. 62, pp. 2530-2539, April 2015.

[8] L. Asiminoaei, P. Rodriguez, F. Blaabjerg, and M. Malinowski, "Reduction of switching losses in active power filters with a new generalized discontinuous- PWM strategy," in *IEEE Transactions on Industrial Electronics*, vol. 55, pp. 467-471, Jan. 2008.

[9] M. H. Ahmed, M. Wang, M. A. S. Hassan, and I. Ullah, "Power loss model and efficiency analysis of three-phase inverter based on SiC MOSFETs for PV applications," in *IEEE Access*, vol. 7, pp. 75768-75781, June 2019.

[10] C. C. Davidson, "Power transmission with power electronics," in *Proc. IEEE 14th Eur. Conf. Power Electron. Appl.*, pp. 1–10, Sep. 2011.

[11] M. Saeedifard, M. Graovac, R. F. Dias, and R. Iravani, "DC power systems: Challenges and opportunities," in *IEEE PES General Meeting*, pp. 1-7, July 2010.

[12] A. Elsayed, A. Mohamed, and O. Mohammed, "DC microgrids and distribution systems: An overview," in *Electric Power Systems Research*, vol. 119. pp. 407-417, 2015.

[13] M. Lonkar, and S. Ponnaluri, “An overview of DC microgrid operation and control,” *Renewable Energy Congress (IREC), 6th International*, pp. 1–6, Mar. 2015.

[14] R. M. Cuzner, and G. Venkataramanan, “The status of DC micro-grid protection,” in *2008 IEEE Industry Applications Society Annual Meeting*, pp. 1-8, Oct. 2008.

[15] J. Aswani, and P. Kanakasabapathy, “Protection of a low-voltage DC ring microgrid system,” in *2016 International Conference on Energy Efficient Technologies for Sustainability (ICEETS)*, pp. 17-22, April 2016.

[16] J.-D. Park, J. Candelaria, L. Ma, and K. Dunn “DC ring-bus microgrid fault protection and identification of fault location”, *IEEE Trans. Power Deliv.*, pp. 2574–2584, 2013.

[17] S. Beheshtaein, R. M. Cuzner, M. Forouzesh, M. Savaghebi, and J. M. Guerrero, “DC microgrid protection: A comprehensive review,” in *IEEE Journal of Emerging and Selected Topics in Power Electronics*, 2019.

[18] L. Zhang, N. Tai, W. Huang, J. Liu, and Y. Wang, “A review on protection of DC microgrids,” *Modern Power Systems and Clean Energy*, pp. 1113-1127, 2018

[19] A. Khorsandi, M. Ashourloo, and H. Mokhtari, “A decentralized control method for a low-voltage DC microgrid,” *IEEE Transactions on Energy Conversion*, vol. 29, no. 4, pp. 793-801, 2014.

[20] K. N. C. Jayasena, D. K. J. S. Jayamaha, and N. W. A. Lidula, A. D. Rajapakse, “Soc

based multi-mode battery energy management system for DC microgrids," in *2019 Moratuwa Engineering Research Conference (MERCon)*, pp. 468-473, July 2019.

[21] H. Kakigano, Y. Miura, and T. Ise, "Distribution voltage control for DC microgrids using fuzzy control and gain-scheduling technique," in *IEEE Transactions on Power Electronics*, vol. 28, pp. 2246-2258, May 2013.

[22] A. Kwasinski, "Advanced power electronics enabled distribution architectures: Design, operation and control," in *8th International Conference on Power Electronics – ECCE Asia*, pp. 1484-1491, 2011.

[23] V. Nougain, V. Nougain, and S. Mishra, "Low-voltage DC ring bus microgrid protection with rolling mean technique," in *2018 IEEMA Engineer Infinite Conference (eTechNxT)*, pp. 1-6, March 2018.

[24] R. Mohanty, and A. K. Pradhan, "Protection of DC and hybrid AC-DC microgrids with ring configuration," in *2017 7th International Conference on Power Systems (ICPS)*, pp. 607-612, Dec. 2017.

[25] L. Strenge, H. Kirchhoff, G. L. Ndow, and F. Hellmann, "Stability of meshed DC microgrids using probabilistic analysis," in *2017 IEEE Second International Conference on DC Microgrids (ICDCM)*, pp. 175-180, June 2017.

[26] A. Prasai, Y. Du, A. Paquette, E. Buck, R. Harley, and D. Divan, "Protection of meshed microgrids with communication overlay," in *2010 IEEE Energy Conversion*

Congress and Exposition, pp. 64-71, Sept. 2010.

[27] T. Vigneysh, N. Kumarappan, and R. Arulraj, "Operation and control of wind/fuel cell based hybrid microgrid in grid connected mode," in *2013 International Multi-Conference on Automation, Computing, Communication, Control and Compressed Sensing (iMac4s)*, pp. 754-758, March 2013.

[28] P. Mathew, S. Madichetty, and S. Mishra, "A multilevel distributed hybrid control scheme for islanded DC microgrids," in *IEEE Systems Journal*, vol. 13, pp. 4200-4207, Dec. 2019.

[29] M. Killi, and S. Samanta, "Modified perturb and observe MPPT algorithm for drift avoidance in photovoltaic systems," in *IEEE Transactions on Industrial Electronics*, vol. 62, pp. 5549-5559, Sept 2015.

[30] A. Yazdani, R. Iravani, *Voltage Sourced Converters in Power Systems: Modeling, Control, and Applications*, Hoboken, N.J.: IEEE Press/Wiley, 2010, pp. 204-244.

[31] D. Singh, A. Agrawal, and R. Gupta, "Power management in solar PV fed microgrid system with battery support," in *2017 14th IEEE India Council International Conference (INDICON)*, pp. 1-6, Dec. 2017.

[32] W. Javed, and D. Chen, "Low voltage DC microgrid protection system - A review," in *2018 53rd International Universities Power Engineering Conference (UPEC)*, pp. 1-6, 2018.

[33] D. Salomonsson, L. Soder, and A. Sannino, “Protection of low-voltage DC microgrid,” in *IEEE Transactions on Power Delivery*, vol. 24, pp. 1045-1053, July 2009.

[34] J. Mohammadi, F. Badrkhani Ajaei, G. Stevens, “DC microgrid grounding strategies,” in *2018 IEEE/IAS 54th Industrial and Commercial Power Systems Technical Conference (I&CPS)*, pp. 1–6, May 2018.

[35] J. C. Das, and R. H. Osman, “Grounding of AC and DC low voltage and medium voltage drive systems,” in *Conference Record of 1997 Annual Pulp and Paper Industry Technical Conference*, pp. 36-47, June 1997.

[36] Y. Wang, Z. Yu, J. He, S. Chen, R. Zeng, and B. Zhang, “Performance of shipboard medium-voltage DC system of various grounding modes under monopole ground fault,” in *IEEE Transactions on Industry Applications*, vol. 51, pp. 5002-5009, 2015.

[37] T. Dragicevic, X. Lu, J. C. Vasquez, and J. M. Guerrero, “DC microgrids-part II: A review of power architectures, applications, and standardization issues,” in IEEE Transactions on Power Electronics, vol. 31, pp. 3528-3549, May 2016.

[38] M. Carminati, and E. Ragaini, “Considerations on DC side grounding configurations of LVDC microgrids”, in *2015 5th International Youth Conference on Energy (IYCE)*, pp. 1-6, 2015.

[39] D. K. J. S. Jayamaha, N. W. A. Lidula, and A. D. Rajapakse, “Ground fault analysis and grounding design considerations in DC microgrids,” in *2018 IEEE 4th Southern*

Power Electronics Conference (SPEC), Dec. 2018.

[40] S. D. A. Fletcher, P. J. Norman, S. J. Galloway and G. M. Burt, "Determination of protection system requirements for dc unmanned aerial vehicle electrical power networks for enhanced capability and survivability," in *IET Electrical Systems in Transportation*, vol. 1, no. 4, pp. 137-147, 2011.

[41] A. Meghwani, S. Chakrabarti, S.C. Srivastava, S.Anand, "Analysis of fault characteristics in DC microgrids for various converter topologies," in *2017 IEEE Innovative Smart Grid Technologies – Asia (ISGT-Asia)*, 2017.

[42] W. A. Martin, C. Deng, D. Fiddiansyah, J. C. Balda, "Investigation of low-voltage solid-state DC breaker configurations for DC microgrid applications," in *2016 IEEE International Telecommunications Energy Conference (INTELEC)*, 2016.

[43] Z. J. Shen, Z. Miao, and A. M. Roshandeh, ''Solid state circuit breakers for DC microgrids: Current status and future trends,'' in *2015 IEEE First International Conference on DC Microgrids (ICDCM)*, pp. 228–233, Jun. 2015.

[44] W. Liu, X. Xiong, H. Yang, K. Feng, and F. Liu, "Combined optimization of SSCB snubber and freewheeling path for surgeless and quick bus fault interruption in low-voltage DC microgrid," in *2016 IEEE Energy Conversion Congress and Exposition (ECCE)*, pp. 1-5, Sept. 2016.

[45] F. Liu, W. Liu, X. Zha, H. Yang, and K. Feng, "Solid-state circuit breaker snubber

design for transient overvoltage suppression at bus fault interruption in low-voltage DC microgrid," in *IEEE Transactions on Power Electronics*, vol. 32, pp. 3007-3021, June 2016.